domains but also cross-linked (e.g., Fab(I) versus HA(II) or Fab(II) versus HA(III)) domains in the complex structure of HA trimer and Fab dimer (see Fig. 1). Thus, we here investigate the interactions of the HA trimer with the Fab dimer by ab initio FMO calculations to quantify the interaction energies at antigenic sites, which would provide a more quantitative measure of how each amino-acid residue is recognized by the Fab antibody.

In the following, we first explain the computational procedure of FMO method in Section 2. Next we show in Section 3 the results for the assessment of the accuracy of calculation, the correlation between hydrogen bonds and IFIE values on the surface of epitopes, and the prediction of amino acid mutations in HA. Concluding remarks are given in Section 4, where we address a possible contribution of the present scheme to the development of influenza vaccine.

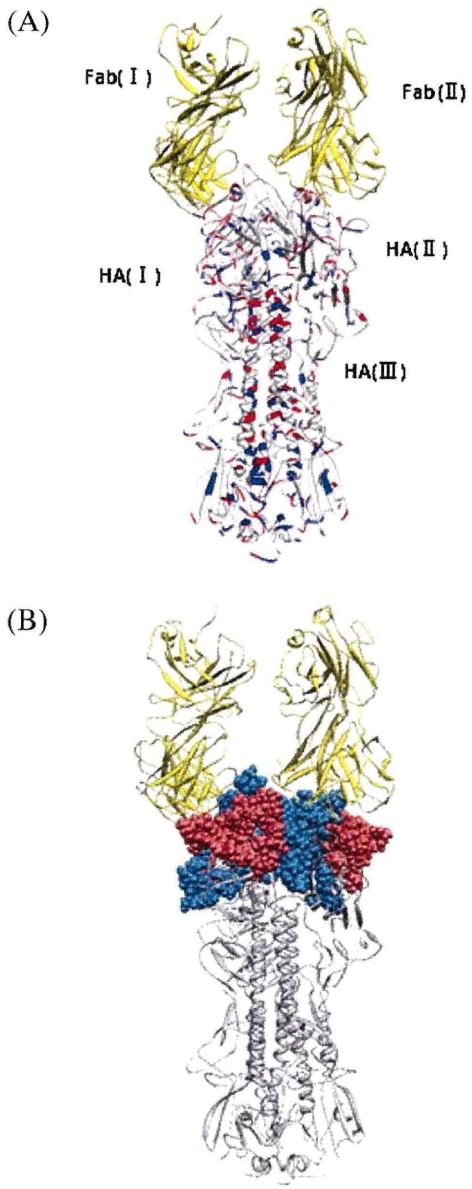

Fig. 1. (A) Visualization of IFIEs between HA trimer (I, II, III) and Fab dimer (I, II) calculated at the FMO-MP2.5/6-31G level. The color represents the sign and strength of the interactions between each residue in the HA trimer and the Fab dimer. For the Fab domain indicated in yellow, the red and blue fragments refer to stabilized and destabilized interactions, respectively, and the deepness of the hue indicates the strength of the interaction. (B) Visualization of antigenic regions A (pink) and B (light blue) by sphere representation. The illustration was created with BioStation Viewer [16]. (For interpretation of the references to color in this figure legend, the reader is referred to the web version of this article.)

2. Materials and computational methods

We consider a complex of HA trimer and Fab dimer that is registered in Protein Data Bank (PDB) with ID code of 1KEN [7]. Each HA monomer has the antigenic regions A–E [1,3], although they are further subdivided and sometimes overlaps of these areas have been noted [13,14]. In particular, the Fab has been observed to be bound with the antigenic regions of A, B and E in electron microscope experiments [15]. The neutralization by antibodies is effective for these regions because they are considered to bind to glycoprotein before it binds to sugar moieties of host cell. In the case of 1KEN, it is observed that the Fab dimer is located over both the antigenic regions of A and B (see Fig. 1 [16]). The antibody HC63 [17] also recognizes the multiple HA monomers primarily through the hydrogen bonds, then suggesting the locations of epitopes containing the residues of numbers 136, 137, 153, 158, 159, 186, 187, 189, 190, 192, 193, 225, 226 (direct-linked), and 126, 128, 162, 163, 165 (cross-linked) [7].

The FMO calculations [18,19] have been performed even for enormous proteins like the complex of HA trimer and Fab dimer [20]. We here employ the Hartree–Fock (HF), the second and third-order Møller–Plesset (MP2 and MP3) perturbation methods for comparison. While the HF method is a rough mean-field approximation, the MP2 and MP3 perturbation methods are employed for the description of electron correlations in the present study, where the latter is expected to correct the tendency of overestimation of stabilization energy in the former [21], but too much. Thus, we can accurately evaluate the binding energy in terms of MP2.5 method which provides a half-and-half mixture of MP2 and MP3 energies [20,21].

It is remarked that the effective fragment–fragment interactions in the FMO scheme [22] are obtained in terms of the inter-fragment interaction energy (IFIE) that is defined as

$$\Delta E_{ij} = (E'_{ij} - E'_i - E'_j) + Tr(\Delta P_{ij} V_{ij}), \tag{1}$$

where ΔP_{ij} is a difference density matrix, V_{ij} is an environmental electrostatic potential for fragment dimer ij from other fragments, and E'_i and E'_{ij} are energies of fragment monomer i and dimer ij without environmental electrostatic potential, respectively. These values ΔE_{ij} then represent the interaction energies of an amino acid residue with a ligand or between amino acid residues because each amino acid is assigned as a single fragment in the present analysis [23–25]. The IFIEs were calculated in this study to analyze the interaction pattern and to estimate the contribution of each residue to binding, as seen in Fig. 1.

It is also convenient to introduce [10,26]

$$\Delta E_{ij}^{\text{total}} = \Sigma_j \Delta E_{ij}, \tag{2}$$

which refers to the contribution of each fragment i to the binding affinity with the domain J containing the grouped residues j. It is noted here that

$$\Delta E_{IJ}^{\text{total}} = \Sigma_i \Delta E_{ij}^{\text{total}} \tag{3}$$

represents the inter-domain interaction between the domain I containing the residues i and the domain J containing the residues j.

The structure of the complex of HA antigen and Fab antibody for the FMO calculations was prepared as follows. Starting with the PDB structure (1KEN), the missing hydrogen atoms were complemented by the MOE (Molecular Operating Environment) software (Chemical Computing Group Inc.). The locations of the hydrogen atoms

were then optimized with the MMFF94x force field. The total numbers of residues and atoms were 2351 and 36,160, respectively. We carried out the FMO-HF (Hartree–Fock), MP2 and MP3 calculations [20] with the basis set 6-31G on the Earth Simulator in Yokohama, as in the previous work [27].

3. Results and discussion

3.1. Analysis of inter–domain interaction energies

We first study the inter–domain interactions in the complex of HA trimer and Fab dimer. As seen in Table 1, the calculated value of the interaction energy between the HA trimer and the Fab dimer is +38.1 kcal/mol at the HF level, while the MP2 and MP3 results have been found to be −163.5 kcal/mol and −127.0 kcal/mol, respectively. The reason why the interaction energy in the HF approximation is positive (repulsive) even though the HA trimer should be attractive to the Fab is that the dispersion energies are not appropriately described. In earlier studies [24,28] with the MP2 method for receptor–ligand systems, it has been demonstrated that the dispersion energies play an important role for describing the interactions of biomacromolecules. We evaluate the interaction energy as −145.3 kcal/mol by the MP2.5 method, which would provide a dependable value. The interaction energies between the HA monomers included in the complex are −1445.5 kcal/mol to −1223.1 kcal/mol in the MP2.5, showing the strong binding. The interaction energies between the Fab monomer and the associated HA monomer for Fab(I)–HA(I) and Fab(II)–HA(II) are −359.9 kcal/mol and −372.0 kcal/mol in the MP2.5, respectively. However, the interactions between the Fab monomer and the other HA monomer, and those between the Fab domains were found to be repulsive. These results suggest that the Fab monomers interact attractively only with the bonding HA monomers. It is then noted that, because of the disulfide bridge at the Fab connection site (not seen explicitly in the structure), there is some affinity instead of steric hindrance in this structure in spite of the repulsive interaction [7].

Table 1
IFIE results (in units of kcal/mol) for inter–domain interactions in the complex of HA-trimer (I, II and III) and Fab-dimer (I and II). The calculated values by the HF, MP2, MP3 and MP2.5 methods with the basis set of 6-31G are shown.

Inter–domain	HF	MP2	MP3	MP2.5
Fab dimer–HA trimer	38.1	−163.5	−127.0	−145.3
Fab(I)–HA(I)	−288.8	−367.0	−352.8	−359.9
Fab(I)–HA(II)	177.5	155.5	144.5	150.0
Fab(I)–HA(III)	134.3	134.3	134.3	134.3
Fab(II)–HA(I)	137.0	137.0	137.0	137.0
Fab(II)–HA(II)	−292.7	−380.4	−363.7	−372.0
Fab(II)–HA(III)	170.8	157.0	159.5	158.2
HA(I)–HA(II)	−1022.4	−1280.4	−1237.1	−1258.7
HA(II)–HA(III)	−981.7	−1245.7	−1200.6	−1223.1
HA(I)–HA(III)	−1189.0	−1469.7	−1421.3	−1445.5
Fab(I)–Fab(II)	210.8	197.7	199.5	198.6
Fab dimer–HA(I)	−151.8	−230.0	−215.8	−222.9
Fab dimer–HA(II)	−115.3	−224.9	−205.0	−214.9
Fab dimer–HA(III)	305.1	291.3	293.8	292.6

IFIE value (kcal/mol).

Table 2
Interaction energies (in units of kcal/mol) between residues calculated with FMO-MP2.5/6-31G method and the donor–acceptor distance (Å) of hydrogen bonds in epitopes. The signatures (A)–(J) are associated with those in Fig. 2. As an exceptional case in the calculation, LEU164 is listed instead of VAL163 in (J) because of the fragmentation at C_α employed in the FMO calculation.

Fab	HA (kcal/mol)	Distance (Å)	Fab	HA (kcal/mol)	Distance (Å)
(A)	ASN137		(B)	ASN137	
ASP104	−22.7	1.39	ASP104	−34.54	1.54
			SER32	−8.70	1.98
	TRP153			TRP153	
ASP104	−4.07		ASP104	−1.86	
(C)	GLY158		(D)	GLY158	
PRO60	−0.42		GLY58	0.88	
ALA61	−0.54		VAL59	0.56	
	SER159			SER159	
PRO60	1.36		GLY58	−5.70	1.86
ALA61	−0.43		VAL59	−11.66	1.80
(E)	SER186		(F)	SER186	
TYR100	−8.27	1.80	TYR100	−5.16	2.51
	THR187			THR187	
TYR100	−2.48		TYR100	−3.02	
	GLN189			GLN189	
TYR109	−9.71	1.52	TYR109	−11.12	1.76
	THR192			THR192	
SER57	−11.11	1.76	SER57	0.73	
	SER193			SER193	
SER57	−0.35		SER57	−15.31	1.60
(G)	THR126		(H)	THR126	
SER31	−1.26		SER31	−0.75	
	THR128			THR128	
THR74	0.14		SER28	−2.89	2.96
SER75	−12.70	1.76			
(I)	PR0162		(J)	PR0162	
GLY26	0.23		SER28	−2.27	
	VAL163			LEU 164	
GLY26	0.63		SER31	−11.44	1.54
TYR27	−11.06	2.03	GLY32	−2.08	
	ASN165			ASN165	
SER31	−0.60		SER31	−6.47	
GLY32	−12.55	1.64	GLY32	−12.05	1.52

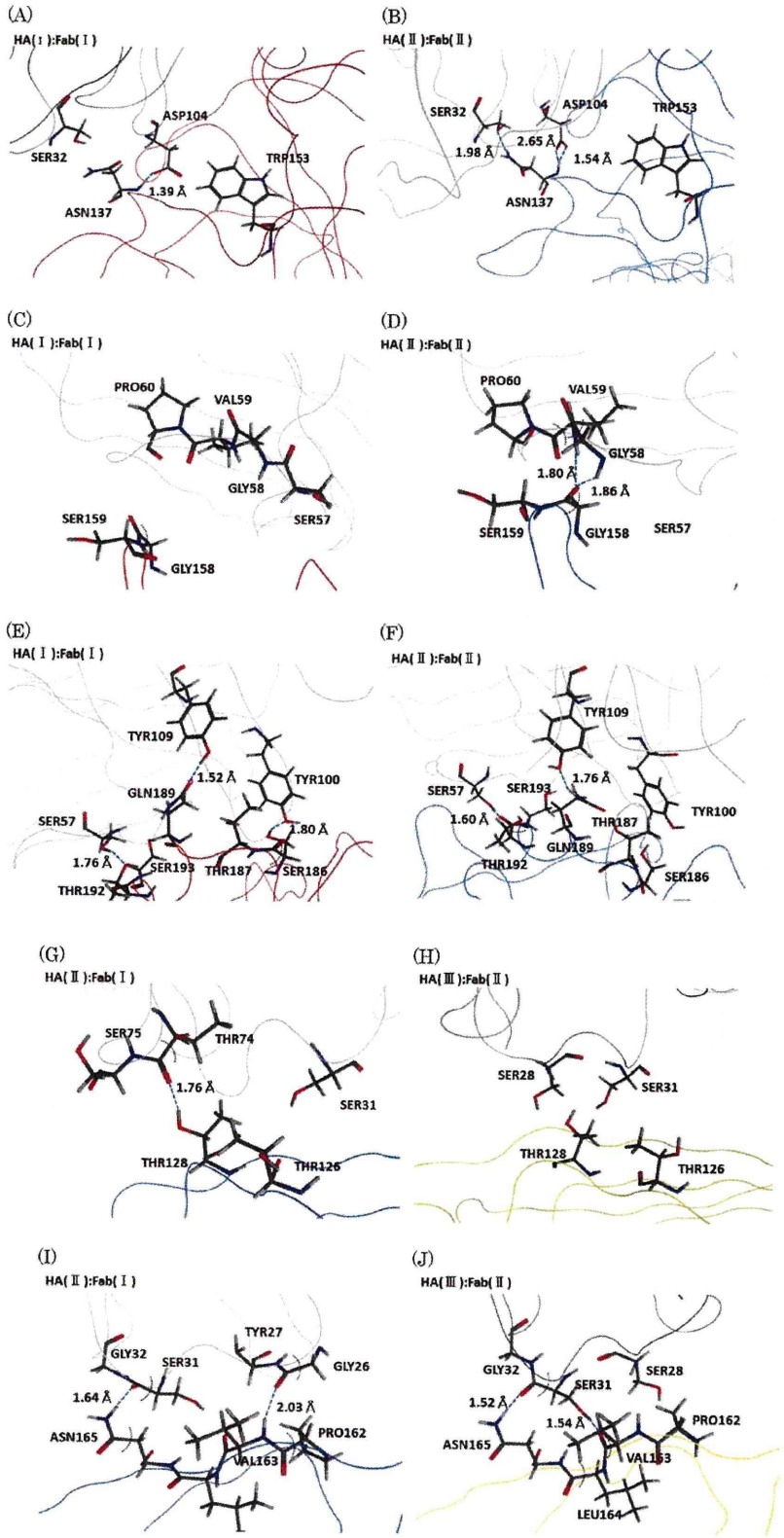

Fig. 2. Details of hydrogen bonds between the Fab and the epitopes in HA. (A)–(F) and (G)–(J) refer to direct-linked and cross-linked domains, respectively; (A), (C), (E) and (B), (D), (F) refer to the interactions between HA(I) and Fab(I) or HA(II) and Fab(II), respectively; Fab in gray, HA(I) in red, HA(II) in blue and HA(III) in yellow. Hydrogen bonds are represented by dotted lines with the distance between donor and acceptor atoms.

Table 3
The hemadsorption activity (p: positive/n: negative; – means no experimental data) and IFIE results (kcal/mol) for the Fab dimer calculated with FMO-MP2.5/6-31G method at the residue sites in antigenic regions A and B of HA. Trimer is the complex of HA(I)–(III), and the mutation years and the types of amino acid after mutation are also listed. The meanings of attached symbols for p sites are as follows. *: Attractive and already mutated site, **: attractive and yet to-be-mutated site, †: repulsive but already mutated site, ††: repulsive and not mutated site.

Region A	p/n	HA(I)	HA(II)	HA(III)	Trimer		Mutation year	Mutation
PHE120	n	0.05	0.39	−0.19	0.24			
ILE121	p	−0.14	−0.76	−0.01	−0.91	*	1995	I-N
THR122	p	0.43	1.24	0.31	1.98	†	1971	T-N
GLU123	–	−46.44	−62.48	−62.62	−171.54			
GLY124	p	0.15	0.24	−0.21	0.19	†	1986, 1996	G-D-S
PHE125	p	−0.72	−1.29	−0.51	−2.52	**		
THR126	p	0.70	−2.74	−0.89	−2.93	*	1973	T-N
TRP127	n	−0.87	−1.15	0.82	−1.20			
THR128	p	0.46	−15.66	−10.86	−26.05	**		
GLY129	n	−0.49	−2.91	−0.39	−3.80			
VAL130	n	0.23	−1.03	0.74	−0.06			
THR131	p	−1.92	−4.16	−1.27	−7.35	*	1987, 2001	T-A-T
GLN132	–	3.02	6.54	4.49	14.05			
ASN133	p	0.86	0.72	1.24	2.81	†	1977, 1991	N-S-D
GLY134	n	−0.13	0.89	−0.20	0.55			
GLY135	p	1.49	−0.03	1.35	2.81	†	1993	G-T
SER136	n	−15.88	−22.56	−0.13	−38.57			
ASN137	p	−24.48	−39.49	−0.54	−64.51	*	1976, 1997	N-Y-S
ALA138	–	−30.89	−31.00	0.89	−61.00			
CYS139	n	−23.09	−19.69	0.11	−42.67			
LYS140	n	21.08	29.32	55.39	105.79		2006	G-I
ARG141	–	33.60	52.72	59.95	146.28			
GLY142	p	−1.65	−3.12	−0.01	−4.78	*	1995	G-R
PR0143	p	−0.43	1.67	0.28	1.52	†	1977	P-S
GLY144	p	−4.71	−3.79	−0.48	−8.97	*	1970, 1982, 1985, 1995	G-D-N-V-R
SER145	p	1.52	−0.65	0.51	1.38	†	1975, 1993, 2004	S-N-K-N
GLY146	p	−6.34	−7.00	−0.48	−13.82	*	1977	G-S
PHE147	p	9.40	7.89	−0.34	16.94	††		
PHE148	n	−3.34	−1.86	0.36	−4.83			
SER149	–	−0.97	−1.42	−1.25	−3.64			
ARG150	–	40.23	55.59	56.94	152.76			
LEU151	n	−0.97	−0.64	−0.46	−2.07			
ASN152	n	3.06	1.05	−0.80	3.31			
TRP153	n	−3.57	−0.17	0.89	−2.84			

Region B	p/n	HA(I)	HA(II)	HA(III)	Trimer		Mutation year	Mutation
LEU154	–	−0.18	−1.72	−1.18	−3.09			
THR155	p	−1.78	−0.29	−0.55	−2.62	*	1971, 1986, 2001	T-Y-H-T
LYS156	p	−24.52	−33.47	82.77	24.78	†	1992, 1995, 2001	E-K-Q-H
SER157	p	0.97	1.02	1.15	3.14	†	1993	S-L
GLY158	p	−1.68	−9.35	−1.47	−12.50	*	1976, 1995	G-E-K
SER159	p	−6.54	−28.09	2.12	−32.52	*	1985, 2002	S-Y-F
THR160	p	3.90	−3.96	0.32	0.25	†	1977	T-K
TYR161	–	1.89	6.83	3.24	11.96			
PR0162	–	−2.61	−3.64	−2.38	−8.64			
VAL163	p	0.93	−4.04	−0.13	−3.24	*	1983	V-A
LEU164	–	0.01	−11.25	−16.43	−27.66			
ASN165	p	−1.16	−2.44	−8.93	−12.53	**		
VAL166	–	0.05	−8.92	−2.13	−11.00			
THR167	–	−0.04	5.16	2.79	7.91			
MET168	–	0.05	−3.88	−3.47	−7.30			
PR0169	–	−0.03	2.79	2.24	5.00			
ASN170	n	0.46	−2.03	−1.61	−3.18			
ASN171	–	−0.29	2.19	1.56	3.46			
ASP172	p	−45.49	−60.16	−59.56	−165.21	*	1976, 1993, 1998	D-G-D-E
ASN173	p	−0.24	0.27	0.04	0.07	†	1982	N-K
PHE174	p	0.32	0.75	0.78	1.85	††		
ASP175	–	−46.03	−49.56	−51.96	−147.55			
LYS176	–	46.24	58.73	59.82	164.80			
LEU177	–	−0.21	1.15	0.72	1.67			
TYR178	n	0.02	−0.76	−0.63	−1.37			
ILE179	n	−0.23	1.01	0.89	1.67			
TRP180	–	0.30	−1.31	−1.86	−2.87			
GLY181	n	0.23	1.07	1.24	2.54			
ILE182	p	−1.04	−1.24	−1.65	−3.94	*	1968	I-V
HIS183	n	2.45	35.21	64.98	102.64			
HIS184	–	33.53	43.09	55.72	132.34			
PR0185	n	6.73	4.00	0.58	11.31			
SER186	–	−15.94	−11.42	0.45	−26.91		1999, 2009	S-G
THR187	–	−12.59	−6.99	−0.02	−19.61			
ASN188	p	5.92	0.53	−1.49	4.96	†	1970	N-D
GLN189	p	−20.65	−28.95	−1.02	−50.61	*	1973, 1987, 1992, 2002	Q-K-R-S-N

Table 3 (*Continued*)

Region B	p/n	HA(I)	HA(II)	HA(III)	Trimer		Mutation year	Mutation
GLU190	–	−11.47	−25.83	−64.32	−101.62		1991	E-D
GLN191	n	5.85	3.99	0.86	10.70			
THR192	p	−12.54	−0.15	−1.35	−14.03	*	1998	T-I
SER193	p	−13.02	−33.20	−3.15	−49.37	*	1972, 1989, 2004	S-N-S-F
LEU194	–	11.86	13.37	−2.04	23.19			
TYR195	–	−0.48	−2.94	−0.50	−3.93			
VAL196	p	−3.64	−6.97	−2.05	−12.66	**		
GLN197	p	−3.37	0.21	1.97	−1.18	*	1977, 1993	Q-R-Q
ALA198	p	1.47	3.85	2.70	8.02	††		
SER199	–	0.67	2.44	1.72	4.82			
GLY200	–	−0.12	−1.41	−0.96	−2.49			
ARG201	–	55.63	55.57	64.96	176.16			
VAL202	n	0.25	−1.09	−1.57	−2.42		2001	V-I
THR203	–	−0.10	1.56	1.55	3.01			
VAL204	n	0.18	−1.48	−1.02	−2.33			

It is known that the MP2 method significantly overestimates the stabilization energy, while the MP3 method underestimates it. To include the higher-order perturbation effects needs the considerable computational costs even by one order. Therefore, we rely on the MP2.5 method [20,21] in the following analysis to represent the interaction energies of amino acid residues, which would provide a quantitative measure.

3.2. Fluctuations in monoclonal antibody recognition

In the analysis of inter-domain interaction energies, we have found that the effect of cross-linked interaction energies should be assessed as well. To gain the information on the molecular recognition by hydrogen bonds in epitopes, we investigate the structures (Fig. 2) and the interaction energy values (Table 2) of the HA antigen–antibody complex. (The signatures (A)–(J) correspond with each other between Fig. 2 and Table 2.)

As seen in Fig. 2(A) and (B) with Table 2(A) and (B), the residue ASP104 in the Fab(I) is bonded by the oxygen and hydrogen atoms to the residue ASN137 in HA(I) with the distance of 1.39 Å, where the calculation result for IFIE is −22.70 kcal/mol. (Hereafter, the distance represents that between hydrogen-bonded donor and acceptor atoms.) On the other hand, the residues ASP104 and SER32 in the Fab(II) are bonded to the residue ASN137 in HA(II) with 1.54 Å and 1.98 Å, respectively; the calculation results for the corresponding IFIEs are −34.54 kcal/mol and −8.70 kcal/mol, respectively. As observed in Fig. 2(C) and (D) with Table 2(C) and (D), the residue ALA61 in Fab(I) interacts attractively with GLY158 and SER159 in HA(I), while both the residues VAL59 and GLY58 in Fab(II) interact with GLY158 and SER159 in HA(II). We also see in Fig. 2(E) and (F) with Table 2(E) and (F) that the interactions between THR192 and SER57 are attractive and repulsive in HA(I)–Fab(I) and HA(II)–Fab(II) complexes, respectively. As an exceptional case in the calculation, as seen in Fig. 2(J) and Table 2(J), LEU164 instead of VAL163 interacts strongly with the Fab by the carbonyl oxygen because of the fragmentation made at C_α, which is employed in the standard FMO recipe [18,19]. In this way, as observed in Fig. 2 and Table 2, the energy values are calculated to be about −5 to −15 kcal/mol with forming the hydrogen bonds shorter than 2 Å, while other electrostatic interaction energy values like the interaction with ASP are larger in magnitude than them. Although the monoclonal antibodies recognize the identical region in HA, the Fab monomers interact with HA trimer with fluctuations. In addition, it is remarked that the present analysis is based on a stable snapshot structure obtained in terms of X-ray crystallographic experiment. Thermal effects at physiological temperatures may thus cause considerable fluctuations in molecular structures and associated interactions of complexes. We should take into account these circumstances in specifying the important amino-acid residues in the HA antigen.

3.3. Hypothetical scheme for predicting the mutations in HA

For the probable mutations of amino acid residues in HA, the following two conditions should be satisfied [10]: that is, the mutant HA should preserve its viral function and also be able to escape the antibody pressure. The former condition is associated with the experimental work carried out by Nakajima et al. [11,12], in which they have extensively introduced single-point mutations in HA and measured the hemadsorption activity of the mutants to assess whether the mutated sites are allowed (positive) or prohibited (negative). The latter condition is associated with the theoretical work in which attractive or repulsive interaction energies with the Fab dimer are evaluated in terms of the values of IFIE sum of the residues in the HA antigenic regions A and B (Table 3). Our hypothesis [10] is that the residues satisfying these two conditions above (i.e., allowed site and attractive interaction) will have a high probability of mutation, which will be examined below through comparison with the historical facts concerning the actual mutations in HA.

Table 3 shows the data regarding the positive(p)/negative(n) sites and the interaction energies with the Fab dimer at the MP2.5/6-31G level for all the amino acid residues in the HA antigenic regions A and B. At first, there are 21 residues of allowed and attractive sites which may be predicted to lead to mutations in our scheme. We see that 17 residues (represented by the symbol *) of them have already been mutated. The other four residues (represented by the symbol **) may be expected to be mutated in future. Next, there are 14 residues at allowed and repulsive sites. Three residues (represented by the symbol ††) of them have not mutated corresponding to our criterion for mutation. However, there are eleven residues (represented by the symbol †) seemingly against our prediction, which are located at the repulsive sites but have experienced the mutations. We will discuss and explain these cases below, where we will categorize them into the charged, polar and hydrophobic residues for quantitative characterization of amino acid residues. In addition, there are a few exceptions concerning the criterion above by the hemadsorption experiment; LYS140 and VAL 202 experienced the mutations in spite of prohibited (n) sites, which may be explained in terms of the differences of mutations between those introduced in the hemadsorption experiment [11,12] and observed actually. Fig. 3 shows the IFIE sums between Fab dimer and each HA monomer in antigenic regions A and B. It is noted that the red bars represent the sites that are allowed (p: positive) and show an attractive interaction

with Fab dimer, which will have a high probability of forthcoming mutation.

As shown in Fig. 3(A), the charged residues LYS156 and ASP172 have possibility to mutate because of positive (allowed) sites and attractive interactions with Fab dimer. In fact, these sites have mutated many times until now. Interaction of LYS156 in HA(III) is very repulsive against Fab dimer because of its non-bonding to Fab dimer with positive charge. However, it shows the large attractive interaction values in HA(I) and (II) so that LYS156 experiences the antibody pressure by the Fab monomers. It is also noted that K156E is favorable for receptor binding and was actually selected under the pressure of antibodies [29]. Interaction energies of charged residues were quantitatively too large due to the neglect of screening effect in the present FMO calculation in vacuo,

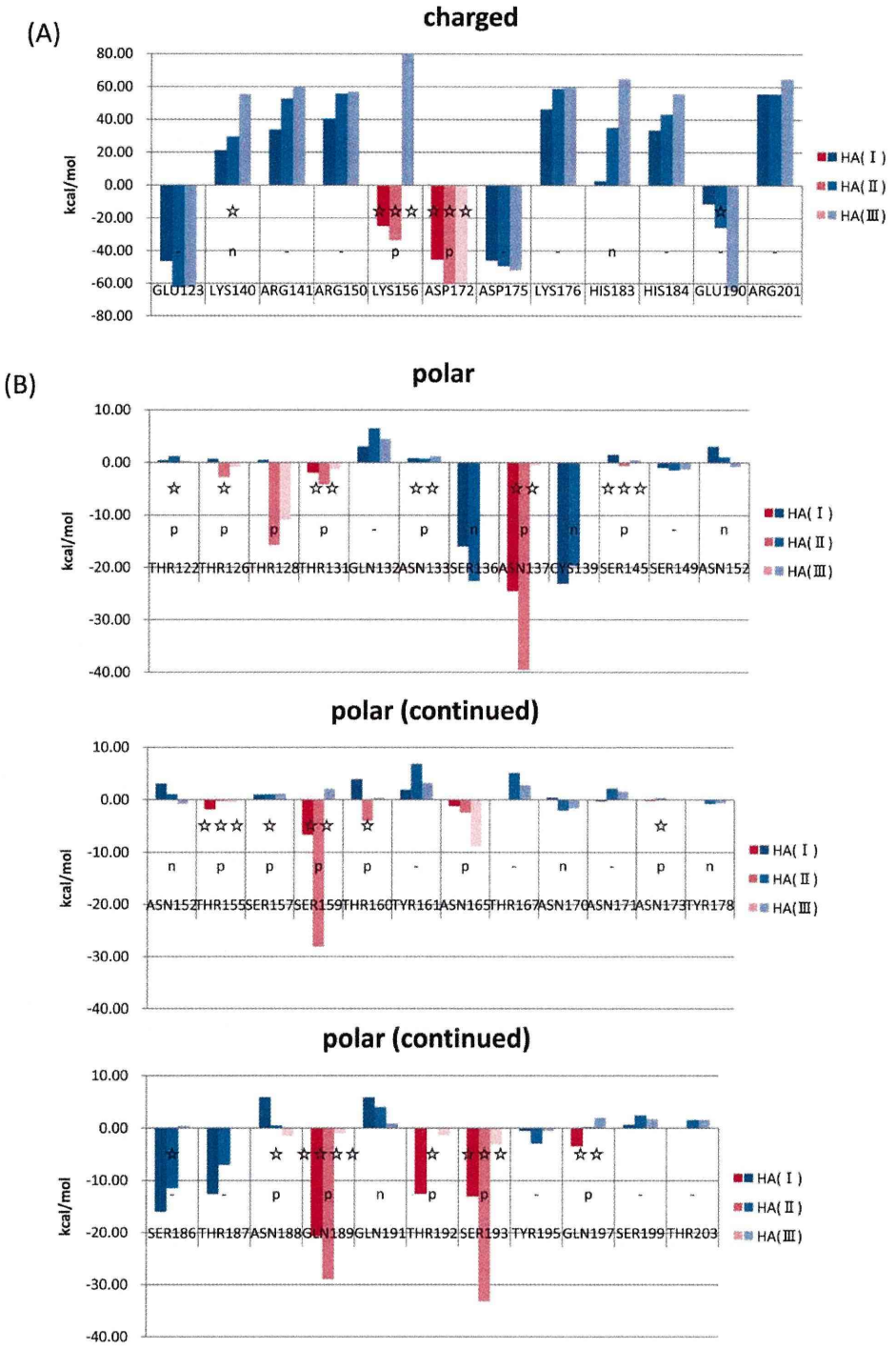

Fig. 3. IFIE sums between Fabs and the residues in the antigenic regions A and B calculated with FMO-MP2.5/6-31G method: (A) charged residues; (B) polar residues; (C) hydrophobic residues. The red bars represent the sites that are allowed (p: positive) and show an attractive interaction with Fab dimer, which will have a high probability of forthcoming mutation; other cases are depicted by the blue bars. The number of stars represents the times of mutations observed already. (For interpretation of the references to color in this figure legend, the reader is referred to the web version of this article.)

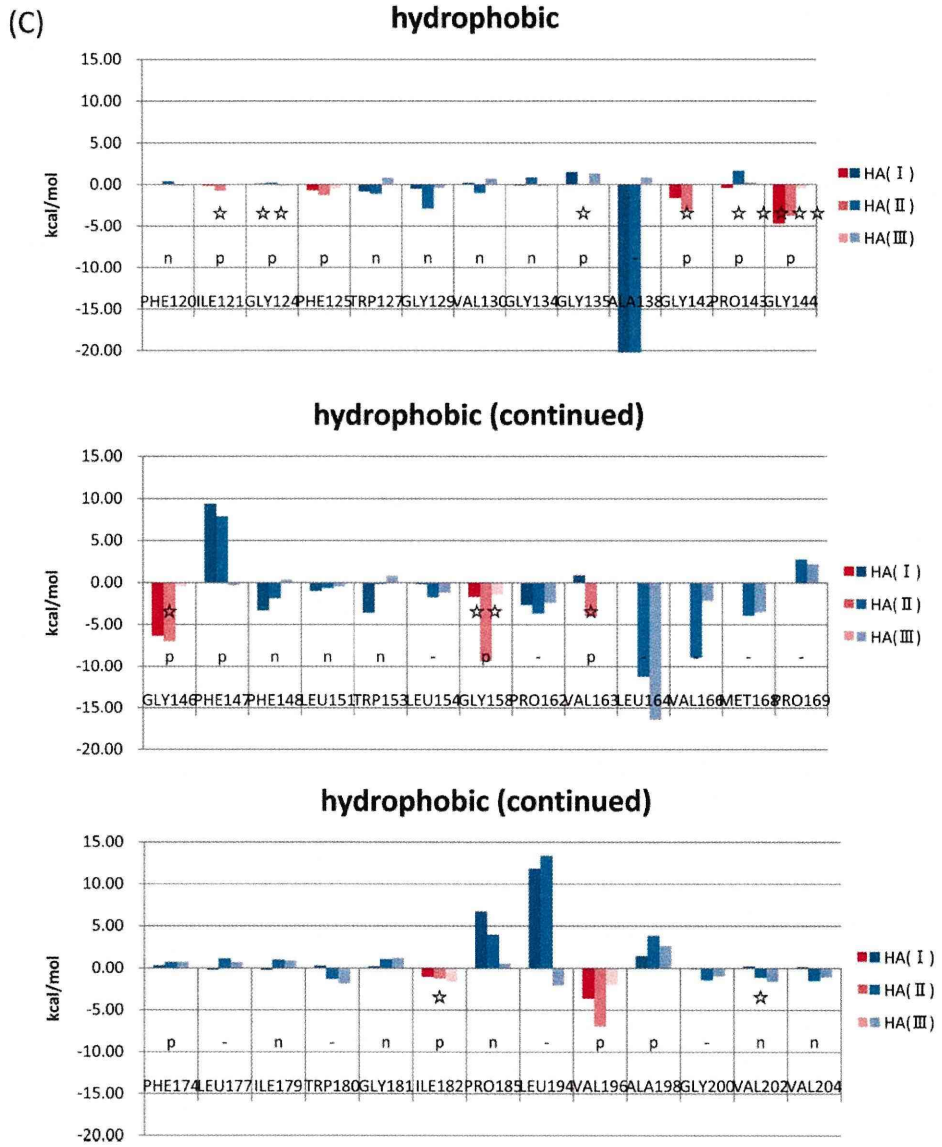

Fig. 3. (*Continued*).

while the comparative features (relative importance and attractive or repulsive interaction) of individual residues are supposed to be described relevantly.

As seen in Fig. 3(B), there are 18 polar residues located at positive (allowed) sites. The eleven sites (126, 128, 131, 137, 155, 159, 165, 173, 189, 192 and 193) are under the antibody pressure apparently, 10 of which have already mutated. The residue 128 may be expected to be mutated in future. Although seven residues (122, 133, 145, 157, 160, 173 and 188) show repulsive interactions with Fab dimer, they have been mutated. The mutations at the 122 and 133 sites have obtained the ability of the oligosaccharide attachment by mutations [30,31]. The residue 133 was actually recognized by monoclonal antibodies until recently [32]. The substitutions N145K and N188D have caused structural changes which allow for the escape from the neutralization by antibodies [33,34]. The substitution S157L allowed for the escape from the antibody HC19 [15]. THR160 receives opposite interactions from multiple Fab monomers. In this case, there are some bonding fluctuations concerning the HA(I) and HA(II) interactions with Fab monomers. We thus suggest that THR160 is under the pressure of an antibody. Because of very small interaction with Fab dimer, the residue ASN173 could not be treated by our prediction scheme.

As observed in Fig. 3(C), the hydrophobic residues show smaller interaction energies than the charged and polar residues. In the present electron-correlated FMO calculations, we can consider the dispersion interactions quantitatively. There are 15 hydrophobic residues located at the allowed (positive) sites. Nine residues (121, 125, 142, 144, 146, 158, 163, 182 and 196) are under the antibody pressure apparently, and seven of them have already been mutated. The residues PHE125 and VAL196 may be expected to be mutated in future. Although three residues (124, 135 and 143) show repulsive interactions with Fab dimer, they have been mutated. The substitution G135R enhances the attractive interaction with glycoprotein [29], and G135T enhances the attractive interaction with sialic acid [35]. The remaining residues GLY124 and PRO143 interact with Fab monomers by 0–1 kcal/mol, which are very weak interactions.

Thus, we have obtained satisfactory results in fair agreement with the historical mutation events, as well as in the earlier study [10]. These results above which were calculated in vacuo, however, ignore the screening effects by solvents [36,37]. Especially,

the IFIE values between charged fragments are substantially overestimated. To cope with this difficulty, although it costs much more, it would be desirable to incorporate the solvation effects into the FMO calculation with, e.g., the Poisson–Boltzmann equation [38]. If this method would be combined with the IFIE calculations, we can evaluate the interaction energies more quantitatively, while careful treatments for the protonation state and the counterions would be required. (Standard aqueous solution pK_a values are assumed in the present analysis.) Further issues to be investigated are the contributions associated with entropy and electronic polarization effects [36,37] in the complex. On the other hand, concerning the calculation levels, it has been observed [28,39] that the relative ordering of the binding energies can be obtained even at such low level as HF/STO-3G. In addition, we can further assess the relative importance of energy values by categorizing the charged, polar and hydrophobic residues, while the interaction energies associated with the hydrophobic residues should be addressed by taking into account the electron correlation effects appropriately.

4. Concluding remarks

The influenza vaccines have been developed mainly against target HA proteins, while it has been difficult to predict forthcoming mutations in HA. We note that only the current calculations cannot detect probable mutations, which may also be associated with the maintenance of HA functions. However, in our combination of computational and experimental methods, to overcome this difficulty, we attempted the detection of possible amino-acid mutations to escape from the antibodies with the aid of the measurement of hemadsorption activities in antigenic regions. As a result, our prediction scheme was found to be consistent with the historical facts of mutations by 83%. (We have picked up the 21 residues of allowed and attractive sites, and two more ones, LYS156 and THR160, showing the attractive interactions at HA monomer level, of which 19 sites have actually mutated.) On the other hand, some mutations unexplained in this analysis were found: however, for example, the substitutions N145K and N188D seemed to induce the structural changes between the HAs of antigenic mutant and the wild type, and G135R and K156E enhanced interactions with glycoprotein under the monoclonal antibodies. Almost all exceptional mutations against our prediction could be explained by considering these previous studies in the literature. Thus the challenge will now be focused on the elucidation of the possible functions of glycoproteins to identify these exceptions. In addition, amino acid changes at more than one residue on the same antigenic site are observed [40,41] for antigenic drift, whose elucidation associated with some cooperative effects may be another challenge. Nonetheless, we expect that this novel computational approach addressed in the present work would be useful for influenza vaccine developments as well.

Acknowledgments

This work was partially supported by the Health and Labour Sciences Research Grants on Emerging and Re-emerging Infectious Diseases (to E.N., No. H22-//Shinko-Ippan-006//) from the Ministry of Health, Labour and Welfare of Japan.

References

[1] J.J. Skehel, D.J. Stevens, R.S. Daniels, A.R. Douglas, M. Knossow, I.A. Wilson, D.C. Wiley, A carbohydrate side chain on hemagglutinins of Hong Kong influenza viruses inhibits recognition by a monoclonal antibody, Proc. Natl. Acad. Sci. U.S.A. 81 (1984) 1779–1783.
[2] R.S. Daniels, A.R. Douglas, J.J. Skehel, D.C. Wiley, Analyses of the antigenicity of influenza haemagglutinin at the pH optimum for virus-mediated membrane fusion, J. Gen. Virol. 64 (1983) 1657–1662.
[3] D.C. Wiley, I.A. Wilson, Structural identification of the antibody-binding site of Hong Kong influenza haemagglutinin and their involvement antigenic variation, Nature 289 (1981) 373–378.
[4] T. Bizebard, B. Gigant, P. Rigolet, B. Rasmussen, O. Diat, S. Bosecke, S. Wharton, J.J. Skehel, M. Knossow, Structure of influenza virus hemagglutinin complexed with a neutralizing antibody, Nature 376 (1995) 92–94.
[5] D. Fleury, B. Barrere, T. Bizebard, R.S. Daniels, J. Skehel, M. Knossow, A complex of influenza hemagglutinin with a neutralizing antibody that binds outside the virus receptor binding site, Nat. Struct. Biol. 6 (1999) 530–534.
[6] D. Fleury, R.S. Daniels, J.J. Skehel, M. Knossow, T. Bizebard, Structural evidence for recognition of a single epitope by two distinct antibodies, Struct. Funct. Gen. 40 (2000) 572–578.
[7] C. Barbey-Martin, B. Gigant, T. Bizebard, L.J. Calder, S.A. Wharton, J.J. Skehel, M. Knossow, An antibody that prevents the hemagglutinin low pH fusogenic transition, Virology 294 (2002) 70–74.
[8] W.D. Kundin, Hong Kong A-2 influenza virus infection among swine during a human epidemic in Taiwan, Nature 228 (1970) 857.
[9] C.A. Russell, The global circulation of seasonal influenza A (H3N2) viruses, Science 320 (2008) 340–346.
[10] K. Takematsu, K. Fukuzawa, K. Omagari, S. Nakajima, K. Nakajima, Y. Mochizuki, T. Nakano, H. Watanabe, S. Tanaka, Possibility of mutation prediction of influenza hemagglutinin by combination of hemadsorption experiment and quantum chemical calculation for antibody binding, J. Phys. Chem. B 113 (2009) 4991–4994.
[11] K. Nakajima, E. Nobusawa, K. Tonegawa, S. Nakajima, Restriction of amino acid change in influenza a virus H3HA: comparison of amino acid changes observed in nature and in vitro, J. Virol. 77 (2003) 10088–10098.
[12] K. Nakajima, E. Nobusawa, A. Nagy, S. Nakajima, Accumulation of amino acid substitutions promotes irreversible structural changes in the hemagglutinin of human influenza AH3 virus during evolution, J. Virol. 79 (2005) 6472–6477.
[13] A.J. Caton, G.G. Brownlee, The antigenic structure of the influenza virus A/PR/8/34 hemagglutinin (HI Subtype) , Cell 31 (1982) 417–427.
[14] D.C. Wiley, The structure and function of the hemagglutinin membrane glycoprotein of inflenza virus, Ann. Rev. Biochem. 56 (1987) 365–394.
[15] N.G. Wrigley, E.B. Brown, R.S. Daniels, A.R. Douglas, J.J. Skehel, D.C. Wiley, Electron microscopy of influenza hemagglutinin-monoclonal antibody complexes, Virology 131 (1983) 308–314.
[16] BioStation Viewer, Available at http://www.fsis.iis.u-tokyo.ac.jp/en/result/software/.
[17] R.S. Daniels, S. Jeffries, P. Yates, G.C. Schild, G.N. Rogers, J.C. Paulson, S.A. Wharton, A.R. Douglas, J.J. Skehel, D.C. Wiley, The receptor-binding and membrane-fusion properties of influenza virus variants selected using anti-hemagglutinin monoclonal antibodies, EMBO J. 6 (1987) 1459–1465.
[18] K. Kitaura, E. Ikeo, T. Asada, T. Nakano, M. Uebayasi, Fragment molecular orbital method: an approximate computational method for large molecules, Chem. Phys. Lett. 313 (1999) 701–706.
[19] D.G. Fedorov, K. Kitaura, Extending the power of quantum chemistry to large systems with the fragment molecular orbital method, J. Phys. Chem. A 111 (2007) 6904–6914.
[20] Y. Mochizuki, K. Yamashita, K. Fukuzawa, K. Takematsu, H. Watanabe, N. Taguchi, Y. Okiyama, M. Tsuboi, T. Nakano, S. Tanaka, Large-scale FMO-MP3 calculations on the surface protein of influenza virus, hemagglutinin (HA) and neuraminidase (NA), Chem. Phys. Lett. 493 (2010) 346–352.
[21] M. Pitoňák, P. Neogrády, J. Černý, S. Grimme, P. Hobza, Scaled MP3 non-covalent interaction energies agree closely with accurate CCSD(T) benchmark data, Chem. Phys. Chem. 10 (2009) 282–289.
[22] K. Kitaura, T. Sawai, T. Asada, T. Nakano, M. Uebayasi, Pair interaction molecular orbital method: an approximate computational method for molecular interactions, Chem. Phys. Lett. 312 (1999) 319–324.
[23] K. Fukuzawa, Y. Komeiji, Y. Mochizuki, A. Kato, T. Nakano, S. Tanaka, Intra- and intermolecular interaction between cyclic-AMP receptor protein and DNA: ab initio fragment molecular orbital study, J. Comput. Chem. 27 (2006) 948–960.
[24] M. Ito, K. Fukuzawa, Y. Mochizuki, T. Nakano, S. Tanaka, Ab initio fragment molecular orbital study of molecular interactions between liganded retinoid X receptor and its coactivator: roles of helix 12 in the coactivator binding mechanism , J. Phys. Chem. B 111 (2007) 3525–3533.
[25] I. Kurisaki, K. Fukuzawa, Y. Komeiji, Y. Mochizuki, T. Nakano, J. Imada, A. Chmielewski, S.M. Rothstein, H. Watanabe, S. Tanaka, Visualization analysis of inter-fragment interaction energies of CRP-cAMP-DNA complex based on the fragment molecular orbital method, Biophys. Chem. 130 (2007) 1–9.
[26] T. Iwata, K. Fukuzawa, K. Nakajima, S. Aida-Hyugaji, Y. Mochizuki, H. Watanabe, S. Tanaka, Theoretical analysis of binding specificity of influenza viral hemagglutinin to avian and human receptors based on the fragment molecular orbital method, Comput. Biol. Chem. 32 (2008) 198–211.
[27] Y. Mochizuki, K. Yamashita, T. Murase, T. Nakano, K. Fukuzawa, K. Takematsu, H. Watanabe, S. Tanaka, Large scale FMO-MP2 calculations on a massively parallel-vector computer , Chem. Phys. Lett. 457 (2008) 396–403.
[28] K. Fukuzawa, Y. Mochizuki, S. Tanaka, K. Kitaura, T. Nakano, Molecular interactions between estrogen receptor and its ligand studied by ab initio fragment molecular orbital method , J. Phys. Chem. B 110 (2006) 16102–16110.
[29] P.A. Underwood, J.J. Skehel, D.C. Willy, Receptor-binding characteristic of monoclonal antibody-selected antigenic variants of influenza virus, J. Virol. 61 (1987) 206–208.
[30] M. Knossow, J.J. Skehel, Variation and infectivity neutralization in influenza, Immunology 119 (2006) 1–7.

[31] Y.P. Lin, V. Gregory, M. Bennett, A. Hay, Recent changes among human influenza viruses, Virus Res. 103 (2004) 47–52.
[32] J. Okada, N. Ohshima, R. Kubota-Koketsu, Y. Iba, S. Ota, W. Takase, T. Yoshikawa, T. Ishikawa, Y. Asano, Y. Okuno, Y. Kurosawa, Localization of epitopes recognized by monoclonal antibodies that neutralized the H3N2 influenza viruses in man, J. Gen. Virol. 92 (2011) 326–335.
[33] D.J. Smith, A.S. Lapedes, J.C. de Jong, T.M. Bestebroer, G.F. Rimmelzwaan, A.D.M.E. Osterhaus, R.A.M. Fouchier, Mapping the antigenic and genetic evolution of influenza virus, Science 305 (2004) 371–376.
[34] M. Knossow, R.S. Daniels, A.R. Douglas, J.J. Skehel, D.C. Willey, Threedimentional structure of an antigenic mutant of the influenza virus haemagglutinin, Nature 311 (1984) 678–680.
[35] A.I. Karasin, M.M. Schutten, L.A. Cooper, C.B. Smith, K. Subbarao, G.A. Anderson, S. Carman, C.W. Olsen, Genetic characterization of H3N2 influenza viruses isolated from pigs in North America, 1977–1999: evidence for wholly human and reassortant virus genotypes, Virus Res. 68 (2000) 71–85.
[36] T. Sawada, D.G. Fedorov, K. Kitaura, Role of the key mutation in the selective binding of avian and human influenza hemagglutinin to sialosides revealed by quantum-mechanical calculations, J. Am. Chem. Soc. 132 (2010) 16862–16872.
[37] T. Sawada, D.G. Fedorov, K. Kitaura, Binding of influenza A virus hemagglutinin to the sialoside receptor is not controlled by the homotropic allosteric effect, J. Phys. Chem. B 114 (2010) 15700–15705.
[38] H. Watanabe, Y. Okiyama, T. Nakano, S. Tanaka, Incorpolation of solvation effects into fragment molecular orbital calculation with the Poisson–Boltzmann equation, Chem. Phys. Lett. 500 (2010) 116–119.
[39] K. Fukuzawa, K. Kitaura, M. Uebayashi, K. Nakata, T. Kaminuma, T. Nakano, Ab initio quantum mechanical study of the binding energies of human estrogen receptor α with its ligands: an application of fragment molecular orbital method, J. Comput. Chem. 26 (2005) 1–10.
[40] I.A. Wilson, N.J. Cox, Structural basis of immune recognition of influenza virus hemagglutinin, Annu. Rev. Immunol. 8 (1990) 737–771.
[41] J.B. Poltkin, J. Dushoff, S.A. Levin, Hemagglutinin sequence clusters and the antigenic evolution of influenza A virus, Proc. Natl. Acad. Sci. U.S.A. 99 (2002) 6236–6268.

Sialic Acid Recognition of the Pandemic Influenza 2009 H1N1 Virus: Binding Mechanism Between Human Receptor and Influenza Hemagglutinin

Kaori Fukuzawa[1,*], Katsumi Omagari[2], Katsuhisa Nakajima[2], Eri Nobusawa[3] and Shigenori Tanaka[4]

[1]*Mizuho Information & Research Institute, Inc., 2-3 Kanda Nishiki-cho, Chiyoda-ku, Tokyo 101-8443, Japan;* [2]*Department of Virology, Medical School, Nagoya City University, 1 Kawasumi, Mizuho-chou, Mizuho-ku, Nagoya 467-8601, Japan;* [3]*National Institute of Infectious Diseases, 4-7-1 Gakuen, Musashimurayama, Tokyo 208-0011, Japan;* [4]*Graduate School of System Informatics, Department of Computational Science, Kobe University, 3-11 Tsurukabuto, Nada, Kobe 657-8501, Japan*

Abstract: Quantum mechanical fragment molecular orbital calculations have been performed for receptor binding of the hemagglutinin protein of the recently pandemic influenza 2009 H1N1 (2009/HIN1pdm), A/swine/Iowa/1930, and A/Puerto Rico/8/1934 viruses to α2-6 linked sialyloligosaccharides, as analogs of human receptors. The strongest receptor binding affinity was observed for the 2009/H1N1pdm. The inter-fragment interaction energy analysis revealed that the amino acid mutation of 2009/H1N1pdm, Ser145Lys, was a major cause of such strong binding affinity. Strong ionic pair interaction between the sialic acid and Lys145 was observed only in the 2009/H1N1pdm, in addition to the hydrogen bond between the sialic acid and Gln226 observed in all the HAs. Therefore, pandemic 2009/H1N1pdm has been found to recognize the α2-6 receptor much stronger than the 1930-swine and 1934-human.

Keywords: Pandemic influenza 2009 H1N1 virus (2009/H1N1pdm), influenza hemagglutinin (HA), sialic acid recognition, fragment molecular orbital (FMO) method, quantum mechanical calculation, sialo-sugar chain.

1. INTRODUCTION

The emergence of the pandemic influenza 2009 H1N1 (2009/H1N1pdm) viruses has become a world-wide health concern. This virus spread rapidly to countries worldwide, suggesting the ease of human-to-human transmission [1-6]. Three kind of membrane proteins exist in the surface of influenza virus: hemagglutinin (HA), neuraminidase (NA), and M2 proton channel which play key role in the processes of viral penetration, viral elution, and viral replication, respectively [7-10]. A series of significant progresses in studying influenza virus and these membrane proteins, both experimentally and theoretically, have been reported recently [1-35]. The infection of influenza occurs via a binding of HA protein to terminal sialic acids of glycoproteins as the cellular receptors for influenza virus. Two types of linkage, α2-6 and α2-3, between sialic acid and the penultimate galactose residues of carbohydrate side chains found in nature. Human influenza viruses recognize the α2-6 linked sialyloligosaccharides (α2-6 receptors), avian viruses recognize the α2-3 linked sialyloligosaccharides (α2-3 receptors), and swine viruses recognize both. Such selectivity characterizes the binding specificity of host receptors [7-9, 11] Therefore, it is important to quantitatively evaluate binding affinity of HA to α2-6 receptors for the understanding of the infection of 2009/H1N1pdm virus to human.

*Address correspondence to this author at the Mizuho Information & Research Institute, Inc., 2-3 Kanda Nishiki-cho, Chiyoda-ku, Tokyo 101-8443, Japan; Tel: +81-3-5281-5271; Fax: +81-3-5281-5331;
E-mail: kaori.fukuzawa@mizuho-ir.co.jp

Since the outbreak in April 2009, several theoretical discussions about the surface membrane proteins for 2009/H1N1pdm virus have been made based on the three-dimensional structures [12-15]. The amino acid sequences of 2009/H1N1pdm virus were published from the NCBI Influenza virus resources [16]. The present study is focused on a HA for 2009/H1N1pdm virus, and its crystal structure was also published from the Protein Data Bank [17]. Although the crystal structures of HA-receptor complex have not been published, several discussions of the receptor binding specificity have been reported from both the viewpoints of sequence and steric structure [5]. The existence of a positively charged 'lysine fence' from Lys133, Lys145, and Lys222, and additional receptor contact with Asp225 have been discussed as a potential key interactions for receptor binding properties of 2009/H1N1pdm HA. In addition to such structural discussions, molecular simulations enable quantitative discussions about molecular interactions between HA and receptors. Here, we have performed quantum mechanical (QM) calculations to analyze the receptor binding of HA based on the 3D-structure of the HA-receptor complex. Because the 2009/H1N1pdm virus contains an HA gene segment from North American swine lineages, and the crystal structure of the complex between A/swine/Iowa/1930 (1930-swine) HA and α2-6 receptor, Sialyllacto-N-tetraose c (LSTc), have been reported [18], we have modeled 3D-structures of the complex between A/California/04/2009 (one of 2009/H1N1pdm virus) HA (Cal4 HA) and α2-6 receptor from those of the 1930-swine HA. We have also calculated binding specificity of two HAs of H1N1 virus with

0929-8665/11 $58.00+.00

human α2-6 receptor: A/swine/Iowa/1930 and A/Puerto Rico/8/1934 HA, the template swine HA and a prototype human HA (1934-human), respectively.

We applied the fragment molecular orbital (FMO) method [36, 37], which has been developed for efficient and accurate QM calculations for biomolecules, to the detailed analysis of molecular interactions between HA and sialo-sugar chain receptor. The FMO method has already been applied for molecular interactions in some influenza HA systems: host receptor specificity of HA [38-40] and HA antigen-antibody system [41-43]. Based on the FMO method and the inter-fragment interaction energy (IFIE) analysis [38, 41, 44] detailed interactions among amino acid residues can be analyzed, and it is also possible to specify the amino acids governing the receptor-binding of HA. Here, we report the FMO results for binding properties between the human α2-6 type receptor and H1HAs of 1930-swine, 2009/H1N1pdm, and 1934-human. Many studies have indicated that computational approaches, such as structural bioinformatics [45-47], molecular docking [48,49], predicting drug-target interaction [50], pharmacophore modelling [51], and binding mechanism studies [38-40, 44, 49, 52] can timely provide very useful information and insights for drug development and hence are widely welcome by science community. The present study is attempted to use the QM FMO calculations to investigate the binding mechanism of human receptor with influenza HA in hopes to provide useful insights not only for revealing true binding mechanisms [24,25,38-40] but also for drug design [26, 28, 31, 53-60] and vaccine developments against influenza virus.

2. MATERIALS AND METHODS

The initial atomic coordinates of the complexes between H1HA and α2-6 receptors were obtained from the Protein Data Bank (PDB ID: 1RVT and 1RVZ for 1930-swine and 1934-human HAs, respectively) [18]. For the 1930-swine HA-receptor complex, 484 amino acid residues and five units of sialo-sugar chain (Sia1-Gal2-GlcNAc3-Gal4-GlcNAc5) were employed for simulations. On the other hand, 483 amino acid residues and three units of sialo-sugar chain (Sia1-Gal2-GlcNAc3) were employed for the 1934-human HA-receptor complex. The molecular geometry of 2009/H1N1pdm HA complex was modeled from those of 1930-swine HA: the side chains of 1930-swine HA amino acid residues were replaced with those of 2009/H1N1pdm (Cal4) HA at the corresponding positions based on the sequence alignment (Fig. (**1**)). Classical molecular mechanics

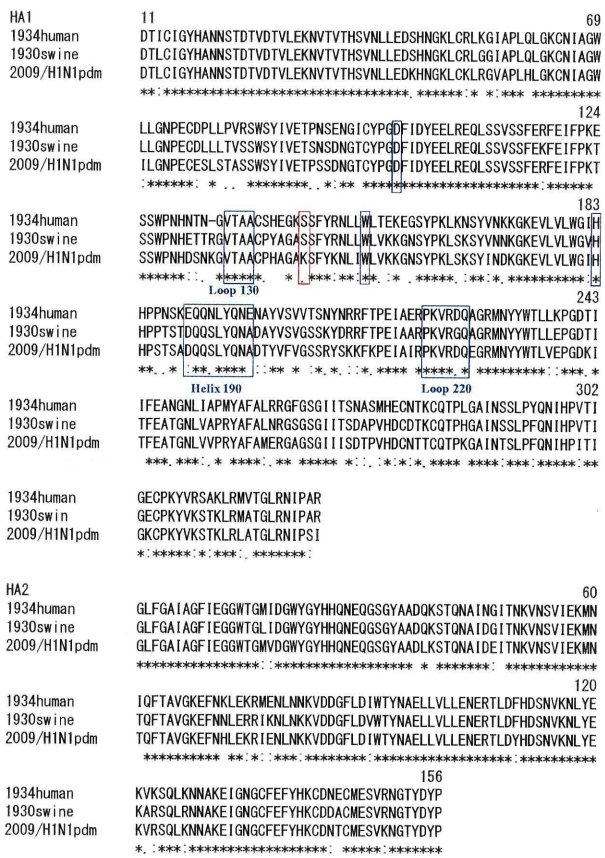

Figure 1. Sequence alignment of 1930-swine, 2009/ H1N1pdm, and 1934-human HAs using the CLUSTALW [69]. '*' indicates fully conserved residue, ':' indicates the residue with strong similarity, and '.' indicates the residue with weaker similarity. Residue numbering is on the basis of H3 HA sequence. The red square indicates 'Ser145Lys' position, The blue squares with rounded corners indicate receptor binding site (Helix 190, Loop130 and Loop220) and conserved residues (Tyr98, Trp153 and His183).

(MM) calculation, including the coordination and minimization of hydrogen and mutated side chain atoms, were performed with parm99SB and GLYCAM_06 force fields using the Amber program [61]. In detail, the system was at first minimized in an implicit water solvent using the Generalized Born (GB) model with force constant of 500 kcal/mol·Å^2 applied to all atoms except for mutated amino acids, followed by all atom minimization in the GB environment. Such modeled geometry for HA portion of 2009/H1N1pdm complex was confirmed to be similar to published PDB crystal structure of free HA [17] (RMSD of backbone atoms in HA1 was 154 Å). Using these geometries, the *ab initio* FMO calculations [36, 37, 62] were carried out under gas-phase conditions at the Hartree-Fock (HF) and Møller-Plesset second order (MP2) levels with the 6-31G* basis set [63,64]. Additionally, the FMO calculations using the spin-component scaled MP2 (SCS-MP2) methods [65, 66] were also carried out in order to modify the overestimation of MP2 binding energies. Note that the geometries of free HA and receptor were fixed at the complexed geometries in the binding energy calculations. The fragmentation of the system was as follows: each amino acid residue of HA, the sialic acid moiety, and each sugar moiety were treated as a single fragment (See Fig. (**2**)) [67]. Therefore, inter-fragment interaction energy (IFIE) analysis can be performed in an amino acid and sugar residue unit. All the FMO calculations were performed with the ABINIT-MP program, and the visualization was carried out with a BioStation Viewer [68]. In the following section, we discuss the results calculated at the FMO-MP2/6-31G* level of theory, unless otherwise stated.

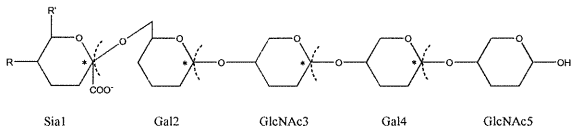

Figure 2. Schematic draw of fragmentation for the sialo-sugar chain. The '*' symbols indicate bond detached atom (BDA).

3. RESULTS

3.1. Binding Energies Between HA and Receptor

In order to estimate binding strength between HA and receptor, both binding energies and IFIEs were analyzed. The binding energies between HA and receptors were calculated by the following equation:

$$\Delta E = E(complex) - \{E(HA) + E(receptor)\} \quad (1)$$

where E(complex), E(HA), and E(receptor) were the total energy of HA-receptor complex, free HA, and free receptor, respectively. As shown in Fig. (**3a**), the overall structures among three HAs of 1930-swine, 2009/H1N1pdm, and 1934 human, were very similar. The calculated binding energies for these HAs were -234, -284, and -155 kcal/mol, respectively at the MP2/6-31G* level (Table **1**), indicating the strongest receptor binding for 2009/H1N1pdm. The SCS-MP2 treatment reduced the overestimation of correlation energies by almost 20%. The sum of IFIE between fragments of HA and those of receptor (IFIE sum) could also be used as the approximate estimation of binding energies [41,44]. Note that similar tendency was observed for IFIE sum values: IFIE sum between HA and receptor with three sugar chains were -263, -329, and -205 kcal/mol for 1930-swine, 2009/H1N1pdm, and 1934-human complexes, respectively (MP2/6-31G*).

3.2. 1930-Swine HA and 2009/H1N1pdm HA

Interactions between sialo-sugar chain and each amino acid residue of HA were compared between 1930-swine HA and 2009/H1N1pdm HA, based on the IFIE analysis. Fig. (**4**) shows numerical representations of IFIE for each residue of HAs with the five sialo-sugar chains receptor, Sia1-Gal2-GlcNAc3-Gal4-GlcNAc5. Residues with strong interactions such as Lys133 – Ala138 and Arg220 – Arg229 were located around the receptor. Some distant residues with negative charge (Asp and Glu) also indicated strong repulsive interactions (Fig. (**4a** and **4b**)). The IFIE results of 2009/ H1N1pdm were also visualized according to color in Fig. (**3e**). Fig. (**4c**) shows the IFIE difference between two HAs, ΔIFIE, and amino acids with the large absolute values of ΔIFIE are also listed in Table **2**. The residue 145 was remarkably stabilized for 2009/H1N1pdm HA with the Ser145Lys substitution (ΔIFIE = 97.4 kcal/mol). The molecular structure at the receptor binding site indicated that the sialic acid form an ionic pair with mutated Lys145 in addition to the hydrogen bond with Gln226 in the 2009/ H1N1pdm HA complex. Their distances were 1.79 and 2.10 Å, respectively (Fig. (**3c**)). For the 1930-swine HA, however, only the hydrogen bond with the Gln226 was observed (1.94 Å), and the Ser 145 was located at the distant position (3.54 Å) (Fig. (**3b**)). Such situation was thought to be a cause of large ΔIFIE value of Ser145Lys. Ala227Glu and Gly225Asp were also found to have large differences, -22.4 and -21.8 kcal/mol, respectively, which is located near the Gal2 moiety of the receptor. No other residue was observed around the receptor with the ΔIFIE of more than 10kcal/mol. Such small differences may originate in the molecular structure of 2009/H1N1pdm HA as a modeling structure from the 1930-swine HA template. As well as the binding energies, the individual IFIE values showed the same tendency among the MP2 and two SCS-MP2 methods.

3.3. 1934-Human HA and 2009/H1N1pdm HA

Interactions between the receptor and HA of both human H1N1 viruses, 2009/H1N1pdm and 1934-human, were also compared. Fig. (**5**) shows numerical representations of IFIE for each residue of HAs with the three sialo-sugar chains receptor, Sia1-Gal2-GlcNAc3. Binding energy of 2009/ H1N1pdm HA with the five sialo-sugar chains receptor was twice larger than that of 1934-human HA with the three sialo-sugar chains receptor (Table **1**). Different lengths of the sugar chains were thought to be one reason of such large difference. Here, interaction analysis with three sialo-sugar chain length of receptor was possible for both HAs based on the IFIE analysis. For the 2009/H1N1pdm, HA-receptor interactions were found to be similar to the case of five sialo-sugar chain receptor. For the 1934-human, residues strongly interacting with the sialo-sugar chain were similar to those of 2009/H1N1pdm, however, some repulsive residues, for instance Glu190, Glu219, Glu142 and Glu156, which were

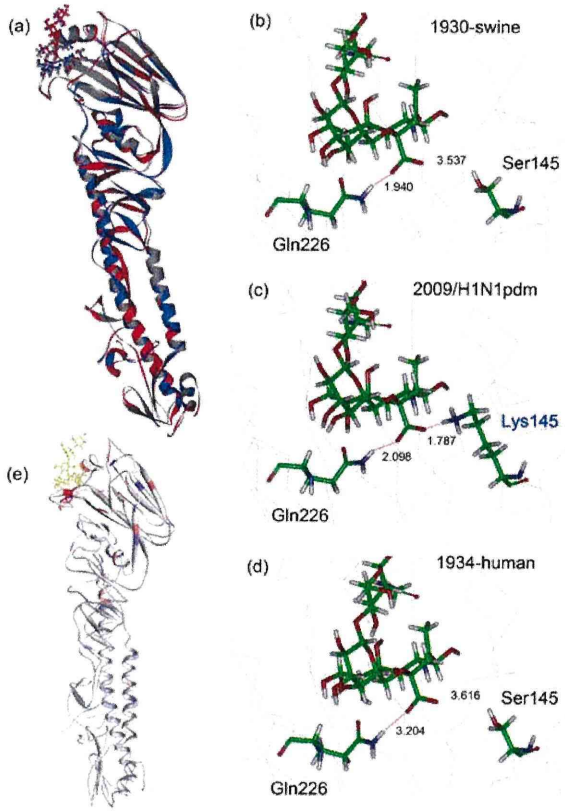

Figure 3. Molecular structures of three HAs **(a-d)**. **(a)** Overall structures of superimposed backbones. **(b-d)** Structures at the sialo-sugar chain receptor binding site: **(b)** 1930-swine, **(c)** 2009/ H1N1pdm, and **(d)** 1934-human. Receptor, Gln226, and Lys145 (Ser145) are displayed with stick representation. The line representation is the Cα backbone. **(e)** Visualized IFIE results calculated at the MP2/6-31G* level for the complex for the 2009/H1N1pdm HA with α2-6 receptor (yellow). Red and blue for residues refer to the interaction energies of stabilization (negative) and destabilization (positive), respectively. The range from -20 to +20 kcal/mol is shown with gradation.

Table 1. Binding Energies and Inter Fragment Interaction Energy (IFIE) Between HA and Receptor

		1930-Swine	2009/H1N1pdm	1934-Human
HF/6-31G*	ΔE	-172.5[a]	-217.8[a]	-106.0[b]
	IFIE[a]	-217.6	-273.4	-
	IFIE[b]	-198.3	-256.1	-145.5
MP2/6-31G*	ΔE	-234.4[a]	-284.2[a]	-154.7[b]
	IFIE[a]	-291.7	-353.9	-
	IFIE[b]	-263.1	-328.7	-204.8
SCS-MP2 (Grimme)	ΔE	-219.9[a]	-268.7[a]	-143.2[b]
	IFIE[a]	-276.5	-337.5	-
	IFIE[b]	-249.8	-313.8	-192.8
SCS-MP2 (Hill)	ΔE	-227.0[a]	-276.3[a]	-149.1[b]
	IFIE[a]	-278.5	-339.6	-
	IFIE[b]	-251.6	-315.9	-193.9

in kcal/mol

a Sia1-Gal2-GlcNAc3-Gal4-GlcNAc5 was used as the receptor

b Sia1-Gal2-GlcNAc3 was used as the receptor

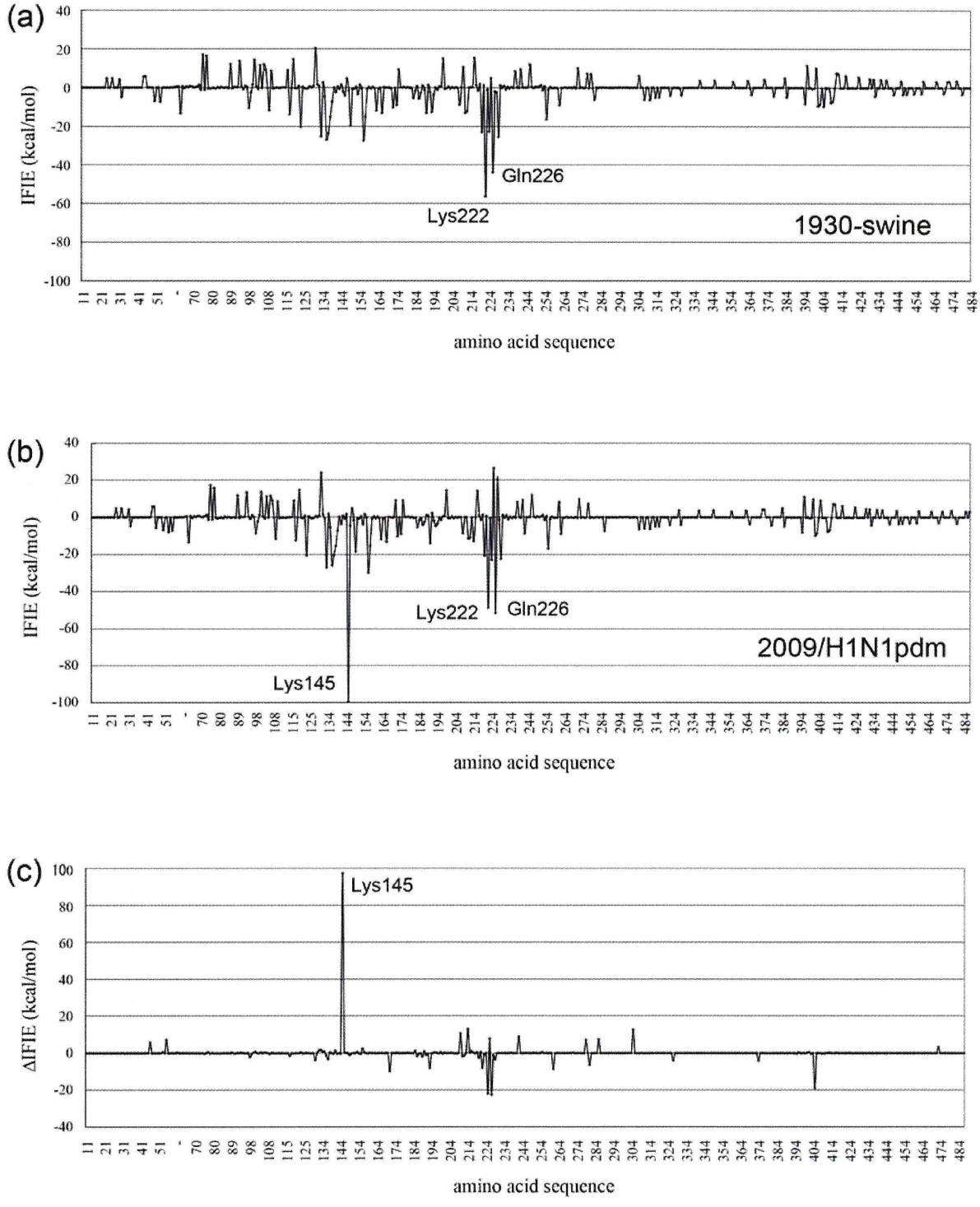

Figure 4. IFIEs between the five sialo-sugar chains receptor and each amino acid residue fragment of HAs: (**a**) 1930-swine, (**b**) 2009/H1N1pdm, and (**c**) their differences (**a-b**).

Table 2. IFIEs Between Five Sialo-Sugar Chains Receptor and each Amino Acid Residue of the HAs

1930-swine		2009/H1N1pdm		
Residue	**IFIE**	**Residue**	**IFIE**	**ΔIFIE**
Ser145	-2.08	Lys145	-99.46	97.4
Thr214	0.16	Lys214	-12.77	12.9
Glu305	6.20	Lys305	-6.39	12.6
Asp210	10.59	Ser210	0.05	10.5
Thr242	0.13	Lys242	-8.66	8.8
Gln226	-43.92	Gln226	-51.66	7.7
His286	0.03	Lys286	-7.27	7.3
Gly60	0.12	Arg60	-6.99	7.1
Asp279	7.10	Asn279	0.12	7.0
Ser46	0.09	Lys46	-5.63	5.7
Lys281	-6.16	Thr281	0.09	-6.2
Lys222	-56.56	Lys222	-48.72	-7.8
Ser193	-12.62	Ser193	-4.70	-7.9
Asn261	-0.34	Glu261	8.19	-8.5
Asn171	-0.44	Asp171	9.17	-9.6
Lys405	-9.66	Glu405	9.14	-18.8
Gly225	4.94	Asp225	26.76	-21.8
Ala227	-1.97	Glu227	20.48	-22.4

substituted residues, were newly observed. ΔIFIE values in Fig. (**5c**) and Table **3** show, again, a high peak at position 145, where different residues were observed between 2009/ H1N1pdm and 1934-human HAs (ΔIFIE = 100.9 kcal/mol). Also, IFIE at the Gln226 was destabilized for 1934-human, ΔIFIE = 25.9 kcal/mol. This is because the hydrogen bond length between sialic acid and Gln226 was observed to be longer (3.20 Å) than 2009/H1N1pdm (Fig. (**3d**)). The other hydrogen bond length of sialic acid with the Ser145 was still long (3.62 Å). Another large ΔIFIE values were observed at the positions where different amino acid residues were found between 1934-human and 2009/H1N1pdm HAs. Compared to the difference between 1930-swine and 2009/H1N1pdm HAs, larger ΔIFIEs (more than 10kcal/mol) were monitored at extensive positions of 2009/H1N1pdm and 1934-human HA.

4. DISCUSSION

Summarizing three HAs, both amino acid sequence and overall backbone structures were very similar (Fig. (**1** and **3a**)). The amino acid sequence of receptor binding site, Helix190 (190-198), Loop130 (135-138), Loop220 (221-228), Tyr98, Trp153, and His183 [38], were highly conserved. However, the side chain structures at the receptor binding site (Fig. (**3b-3d**)) indicated that the sialic acid formed hydrogen bond with the Gln226 for all three HAs but an additional ionic pair bond between residue Lys145 and the sialic acid was found only for 2009/H1N1pdm HA. Both 1930-swine and 1934-human HAs have Ser145, which formed a weak or no hydrogen bond with the sialic acid. Most of 2009/ H1N1pdm HA has Lys at the position 145. IFIE analysis provided quantitative theoretical evidence for these interactions, and such hydrogen bonds and ionic pair networks made strong bindings between 2009/H1N1pdm HA and human-type receptor. Therefore, the current swine-origin pandemic virus has been found to recognize the α2-6 receptors (human type) much stronger than 1934-human, a prototype human virus, and 1930-swine, an ancestor of the 2009/ H1N1pdm virus.

Furthermore, together with the discussions based on the steric structures [5], IFIE analysis provides in-depth information about HA-receptor interaction. Sum of IFIE values between α2-6 receptor (three sialo-sugar chain length) and a positively charged 'lysine fence'-which are constructed from Lys133, Lys145, and Lys222 in 2009/H1N1pdm (Cal4); from Arg133, Ser145, and Lys222 in 1930-swine; and from gap at position 133 (see Fig. (**1**)), Ser145, and Lys222 in 1934-human-were -184.7, -89.0, and -60.4 kcal/mol, respectively. Clearly, interactions between such 'lysine fence' of 2009/H1N1pdm and α2-6 receptor stabilize their binding.

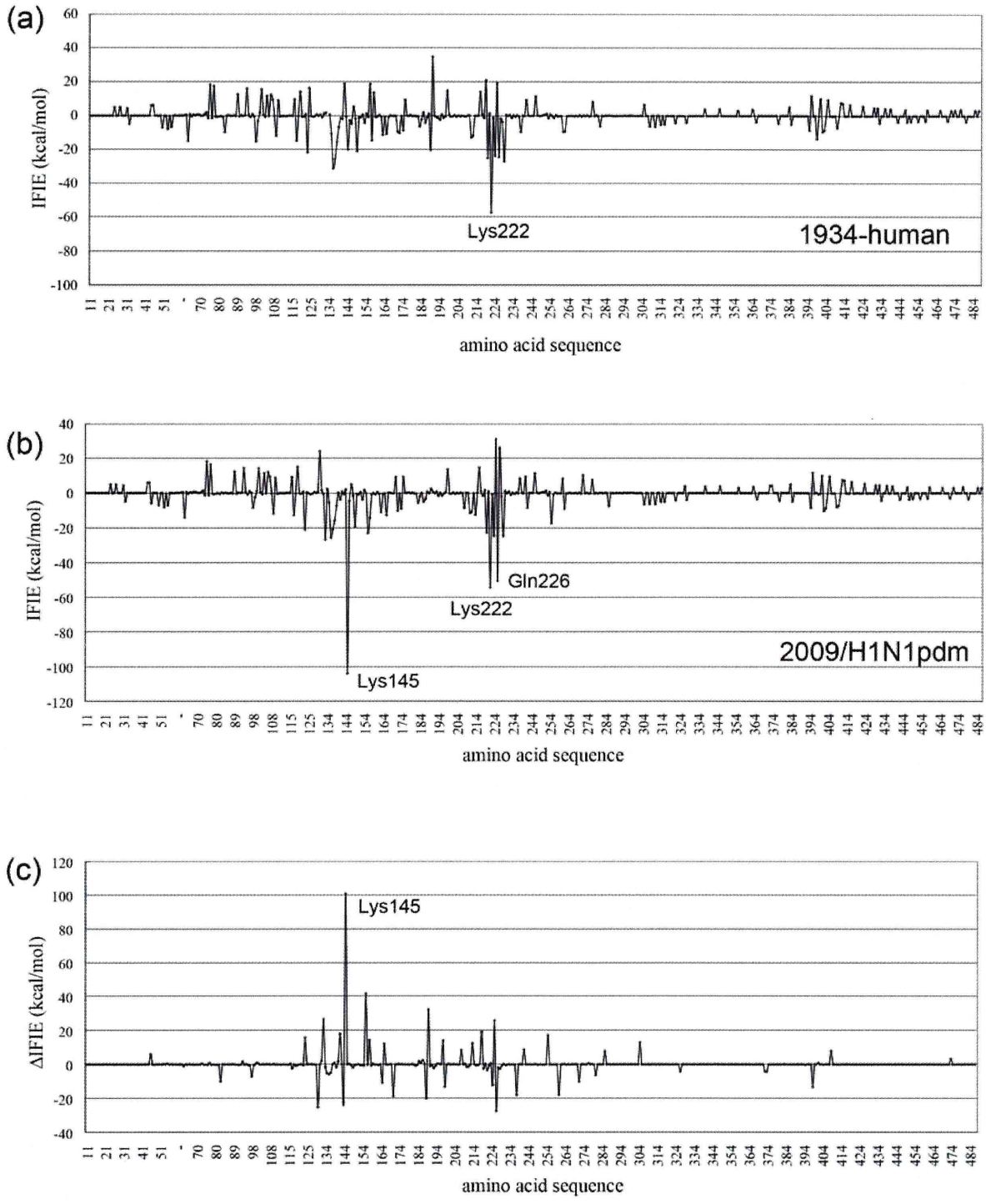

Figure 5. IFIEs between the three sialo-sugar chains receptor and each amino acid residue fragment of HAs: (**a**) 1934-human, (**b**) 2009/H1N1pdm, and (**c**) their differences (**a-b**).

Table 3. IFIEs Between Three Sialo-Sugar Chains Receptor and each Amino Acid Residue of the HAs

1934-Human		2009/H1N1pdm		
Residue	**IFIE**	**Residue**	**IFIE**	**ΔIFIE**
Ser145	-2.88	Lys145	-103.82	100.9
Glu156	18.80	Lys156	-22.80	41.6
Glu190	34.82	Asp190	2.51	32.3
Gln226	-24.49	Gln226	-50.37	25.9
Glu219	20.83	Ile219	1.71	19.1
Glu142	18.90	Ala142	0.86	18.0
Met255	-0.02	Arg255	-17.18	17.2
Glu124	16.23	Thr124	0.46	15.8
Glu158	13.49	Gly158	-0.87	14.4
Glu198	14.81	Ala198	0.71	14.1
Glu305	6.46	Lys305	-6.54	13.0
Thr214	0.01	Lys214	-12.45	12.5
Asn166	-0.78	Lys166	-12.87	12.1
Arg82	-9.74	Ser82	0.37	-10.1
Asn272	0.20	Asp272	10.33	-10.1
Lys165	-10.86	Ser165	-0.14	-10.7
Asp225	19.10	Asp225	31.18	-12.1
Asn199	0.55	Asp199	13.59	-13.0
Lys399	-13.78	His399	-0.55	-13.2
Arg261	-9.52	Glu261	8.30	-17.8
Lys238	-9.57	Glu238	8.37	-17.9
Lys171	-9.41	Asp171	9.18	-18.6
Lys189	-19.99	Ala189	-0.16	-19.8
Lys144	-20.03	Ala144	2.02	-22.1
Asn(130+1)	-0.90	Asp(130+1)	24.15	-25.1
Ala227	-1.74	Glu227	25.66	-27.4

However, additional contact of 2009/H1N1pdm with α2-6 receptor by Asp225 destabilizes their binding; IFIE between α2-6 receptor and Asp225 (2009/H1N1pdm), Gly225 (1930-swine), and Asp225 (1934-human) were 31.2, 19.1, and 5.1 kcal/mol, respectively (See Table **S2** for detailed IFIE values). Such repulsive interaction may not exist for the complex between 2009/H1N1pdm and α2-3 receptor [5], which may cause their greater affinity.

5. CONCLUSION

In terms of the quantum mechanical FMO analysis, we have quantitatively analyzed the binding affinity of HAs (2009/H1N1pdm, 1930-swine, and 1934-human) to α2-6 receptors, as analogs of human receptors. Through the IFIE analysis based on the FMO calculations, we could also specify and characterize important residues which would play an essential role in the binding specificity between HA and a receptor; especially the Lys145 was found to be an important characteristic of the 2009 pandemic virus HA.

ACKNOWLEDGMENTS

The authors thank Prof. Yuji Mochizuki, Dr. Tatsuya Nakano, and Mr. Kazutomo Takematsu for discussions about FMO calculations. The authors also thank Mr. Katsumi Yamashita, Dr. Yoshio Okiyama, and Mr. Akifumi Kato for development of ABINIT-MP and BioStation Viewer codes. This work was primarily supported by the "Core Research for Evolutional Science and Technology" project of the Ja-

pan Science and Technology Agency (JST-CREST). A part of this research was also carried out in conjunction with the "Research and Development of Innovative Simulation Software (RISS)" project supported by the Ministry of Education, Culture, Sports, Science, and Technology (MEXT).

SUPPLEMENTARY MATERIAL

Supplementary material is available on the publishers Web site along with the published article.

REFERENCES

[1] Neumann, G.; Noda, T.; Kawaoka, Y. Emergence and pandemic potential of swine-origin H1N1 influenza virus. *Nature*, **2009**, *459*, 931-939.

[2] Smith, G. J. D.; Vijaykrishna, D.; Bahl, J.; Lycett, S. J.; Worobey, M.; Pybus, O. G.; Ma, S. K.; Cheung, C. L.; Raghwani, J.; Bhatt, S.; Malik Peiris, J. S.; Guan, Y.; Rambaut, A. Origins and evolutionary genomics of the 2009 swine-origin H1N1 influenza A epidemic. *Nature*, **2009**, *459*, 1122-1126.

[3] Garten, R. J.; Davis, C. T.; Russell, C. A.; Shu, B.; Lindstrom, S.; Balish, A.; Sessions, W. M.; Xu, X.; Skepner, E.; Deyde, V.; Okomo-Adhiambo, M.; Gubareva, L.; Barnes, J.; Smith, C. B.; Emery, S. L.; Hillman, M. J.; Rivailler, P.; Smagala, J.; de Graaf, M.; Burke, D. F.; Fouchier, R. A. M.; Pappas, C.; Alpuche-Aranda, C. M.; López-Gatell, H.; Olivera, H.; López, I.; Myers, C. A.; Faix, D.; Blair, P. J.; Yu, C.; Keene, K. M.; Dotson Jr., P. D.; Boxrud, D.; Sambol, A. R.; Abid, S. H.; St. George, K.; Bannerman, T.; Moore, A. L.; Stringer, D. J.; Blevins, P.; Demmler-Harrison, G. J.; Ginsberg, M.; Kriner, P.; Waterman, S.; Smole, S.; Guevara, H. F.; Belongia, E. A.; Clark, P. A.; Beatrice, S. T.; Donis, R.; Katz, J.; Finelli, L.; Bridges, C. B.; Shaw, M.; Jernigan, D. B.; Uyeki, T. M.; Smith, D. J.; Klimov, A. I.; Cox, N. J. Antigenic and genetic characteristics of swine-origin 2009 A(H1N1) influenza viruses circulating in humans. *Science*, **2009**, *325*, 197-201.

[4] Schnitzler, S. U.; Schnitzler, P. An update on swine-origin influenza virus A/H1N1: a review. *Virus Genes*, **2009**, *39*, 279-292.

[5] Soundararajan, V.; Tharakaraman, K.; Raman, R.; Raguram, S.; Shriver, Z.; Sasisekharan, V.; Sasisekharan, R. Extrapolating from sequence—the 2009 H1N1 'swine' influenza virus. *Nat. Biotech.*, **2009**, *27*, 510-513.

[6] Ito, T.; Couceiro, J. N. S. S.; Kelm, S; Baum, L. G.; Krauss, S.; Castrucci, M. R.; Donatelli, I.; Kida, H.; Paulson, J. C.; Webster, R. G.; Kawaoka Y. Molecular basis for the generation in pigs of influenza a viruses with pandemic potential. *J. Virol.*, **1998**, *72*, 7367-7373.

[7] Skehel, J. J.; Wiley, D.C. Receptor binding and membrane fusion in virus entry: the influenza hemagglutinin. *Ann. Rev. Biochem.*, **2000**, *69*, 531-569.

[8] Horimoto, T.; Kawaoka, Y. Influenza: lessons from past pandemics, warnings from current incidents, *Nat. Rev. Microbiol.*, **2005**, *3*, 591-600.

[9] Neumann, G.; Kawaoka, Y. Host range restriction and pathogenicity in the context of influenza pandemic. *Emerg. Infect. Dis.*, **2006**, *12*, 881-886.

[10] Pielak, R. M.; Chou, J. J. Influenza M2 proton channels. *Biochim. Biophys. Acta*, **2010**, 10.1016/j.bbamem.2010.1004.1015.

[11] Suzuki, Y. Sialobiology of influenza: molecular mechanism of host range variation of influenza viruses. *Biol. Pharm. Bull.*, **2005**, *28*, 399-408.

[12] Du, Q. S.; Wang, S. Q.; Huang, R. B.; Chou, K. C. Computational 3D structures of drug-targeting proteins in the 2009-H1N1influenza A virus. *Chem. Phys. Lett.*, **2010**, *485*, 191-195.

[13] Wang, J. F.; Chou, K. C. Insights from studying the mutation-induced allostery in the M2 proton channel by molecular dynamics. *Protein Eng Des Sel.*, **2010**, *23*, 663-666.

[14] Wang, J. F.; Wei, D. Q.; Chou, K. C. Insights from investigating the interactions of adamantane-based drugs with the M2 proton channel from the H1N1 swine virus. *Biochem. Biophys. Res. Commun.*, **2009**, *388*, 413-417.

[15] Wang, S. Q.; Du, Q. S.; Huang, R. B.; Zhang, D. W.; Chou, K. C. Insights from investigating the interaction of oseltamivir (Tamiflu) with neuraminidase of the 2009 H1N1 swine flu virus. *Biochem. Biophys. Res. Commun.* **2009**, *386*, 432-436.

[16] NCBI. Influenza Virus Resource. http://www.ncbi.nlm.nih.gov/genomes/FLU/FLU.html

[17] Xu, R.; Ekiert, D. C.; Krause, J. C.; Hai, R.; Crowe Jr., J. E.; Wilson I. A. Structural Basis of Preexisting Immunity to the 2009 H1N1 Pandemic Influenza Virus. *Science*, **2010**, *328*, 357-360.

[18] Gamblin, S. J.; Haire, L. F.; Russell, R. J.; Stevens, D. J.; Xiao, B.; Ha, Y.; Vasisht, N.; Steinhauer, D. A.; Daniels, R. S.; Elliot, A.; Wiley, D. C.; Skehel J. J. The structure and receptor binding properties of the 1918 influenza hemagglutinin. *Science*, **2004**, *303*, 1838-1842.

[19] Schnell, J. R.; Chou, J. J. Structure and mechanism of the M2 proton channel of influenza A virus. *Nature*, **2008**, *451*, 591-595.

[20] Pielak, R. M.; Jason R. Schnell, J. R.; Chou, J. J. Mechanism of drug inhibition and drug resistance of influenza A M2 channel. *Proc. Natl. Acad. Sci. USA*, **2009**, *106*, 7379-7384.

[21] Wang, J.; Pielak, R. M.; McClintock, M. A.; Chou, J. J. Solution structure and functional analysis of the influenza B proton channel. *Nat. Struct. Mol. Biol.*, **2009**, *16*, 1267-1271.

[22] Pielak, R. M.; Chou, J. J. Solution NMR structure of the V27A drug resistant mutant of influenza A M2 channel. *Biochem. Biophys. Res. Commun.*, **2010**, *401*, 58-63.

[23] Pielak, R. M.; Chou, J. J. Flu channel drug resistance: a tale of two sites. *Protein Cell*, **2010**, *1*, 246-258.

[24] Huang, R. B.; Du, Q. S.; Wang, C. H.; Chou, K. C. An in-depth analysis of the biological functional studies based on the NMR M2 channel structure of influenza A virus. *Biochem. Biophys. Res. Comm.*, **2008**, *377*, 1243-1247.

[25] Du, Q. S.; Huang, R. B.; Wang, C. H.; Li, X. M.; Chou, K. C. Energetic analysis of the two controversial drug binding sites of the M2 proton channel in influenza A virus. *J. Theor. Biol.*, **2009**, *259*, 159-164.

[26] Wei, H.; Wang, C. H.; Du, Q. S.; Meng, J.; Chou, K. C. Investigation into adamantane-based M2 inhibitors with FB-QSAR. *Med. Chem.*, **2009**, *5*, 305-317.

[27] Wang, N. X.; Zheng, J. J. Computational studies of H5N1 influenza virus resistance to oseltamivir. *Protein Sci.*, **2009**, *18*, 707-715.

[28] Wei, D. Q.; Du, Q. S.; Sun, H.; Chou, K. C. Insights from modeling the 3D structure of H5N1 influenza virus neuraminidase and its binding interactions with ligands. *Biochem. Biophys. Res. Comm.*, **2006**, *344*, 1048-1055.

[29] Wang, S. Q.; Du, Q. S.; Chou, K. C. Study of drug resistance of chicken influenza A virus (H5N1) from homology-modeled 3D structures of neuraminidases. *Biochem. Biophys. Res. Comm.*, **2007**, *354*, 634-640.

[30] Du, Q. S.; Wang, S. Q.; Chou, K. C. Analogue inhibitors by modifying oseltamivir based on the crystal neuraminidase structure for treating drug-resistant H5N1 virus. *Biochem. Biophys. Res. Comm.*, **2007**, *362*, 525-531.

[31] Gong, K.; Li, L.; Wang, J. F.; Cheng, F.; Wei, D. Q.; Chou, K. C. Binding mechanism of H5N1 influenza virus neuraminidase with ligands and its implication for drug design. *Med. Chem.*, **2009**, *5*, 242-249.

[32] Du, Q. S.; Huang, R. B.; Wang, S. Q.; Chou, K. C. Designing inhibitors of M2 proton channel against H1N1 swine influenza virus. *PLoS One*, **2010**, *5*, e9388.

[33] Du, Q. S.; Huang, R. B.; Wang, C. H.; Li, X. M.; Chou, K. C. Energetic analysis of the two controversial drug binding sites of the M2 proton channel in influenza A virus. *J. Theor. Biol.*, **2009**, *259*, 159-164.

[34] Wei, H.; Wang, C. H.; Du, Q. S.; Meng, J.; Chou, K. C. Investigation into adamantane-based M2 inhibitors with FB-QSAR. *Med. Chem.*, **2009**, *5*, 305-317.

[35] Wang, S. Q.; Cheng, X. C.; Dong, W. L.; Wang, R. L.; Chou, K. C. Three new powerful Oseltamivir derivatives for inhibiting the neuraminidase of influenza virus. *Biochem. Biophys. Res. Commun.*, **2010**, *401*, 188-191.

[36] Fedorov, D. G.; Kitaura, K. Eds.; The Fragment Molecular Orbital Method: Practical Applications to Large Molecular Systems; CRC Press: Boca Raton, FL, **2009**.

[37] Fedorov, D.G.; Kitaura, K. Extending the Power of Quantum Chemistry to Large Systems with the Fragment Molecular Orbital Method. *J. Phys. Chem.*, **2007**, *A 111*, 6904-6914.

[38] Iwata, T.; Fukuzawa, K.; Nakajima, K.; Aida-Hyugaji, S.; Mochizuki, Y.; Watanabe, H.; Tanaka, S. Theoretical analysis of binding specificity of influenza viral hemagglutinin to avian and human receptors based on the fragment molecular orbital method Comp. *Biol. Chem.,* **2008**, *32*, 198-211.

[39] Sawada, T.; Hashimoto, T., Nakano, H.; Suzuki, T.; Ishida, H.; Kiso, M. Why does avian influenza A virus hemagglutinin bind to avian receptor stronger than to human receptor? Ab initio fragment molecular orbital studies. *Biochem. Biophys. Res. Comm.,* **2006**, *351*, 40-43.

[40] Sawada, T.; Hashimoto, T.; Tokiwa, H.; Suzuki, T.; Nakano, H.; Ishida, H.; Kiso, M.; Suzuki, Y. Ab initio fragment molecular orbital studies of influenza virus hemagglutinin–sialosaccharide complexes toward chemical clarification about the virus host range determination. *Glycoconj. J.,* **2008**, *25*, 805-815.

[41] Takematsu, K.; Fukuzawa, K.; Omagari, K.; Nakajima, S.; Nakajima, K.; Mochizuki, Y.; Nakano, T.; Watanabe, H.; Tanaka, S. Possibility of Mutation Prediction of Influenza Hemagglutinin by Combination of Hemadsorption Experiment and Ab Initio Calculation for Antibody Binding. *J. Phys. Chem.,* **2009**, *B 113,* 4991-4994.

[42] Mochizuki, Y.; Yamashita, K.; Murase, T.; Nakano, T.; Fukuzawa, K.; Takematsu, K.; Watanabe, H.; Tanaka, S. Large scale FMO-MP2 calculations on a massively parallel-vector computer. *Chem. Phys. Lett.,* **2008**, *457*, 396-403.

[43] Mochizuki, Y.; Yamashita, K.; Fukuzawa, K.; Takematsu, K.; Watanabe, H.; Taguchi, N.; Okiyama, Y.; Tsuboi, M.; Nakano, T.; Tanaka, S. Large-scale FMO-MP3 calculations on the surface proteins of influenza virus, hemagglutinin (HA) and neuraminidase (NA). *Chem. Phys. Lett.,* **2010**, *493*, 346-352.

[44] Fukuzawa, K.; Mochizuki, Y.; Tanaka, S.; Kitaura, K.; Nakano, T. Molecular Interactions between Estrogen Receptor and Its Ligand Studied by the Ab Initio Fragment Molecular Orbital Method. *J. Phys. Chem. B,* **2006**, *110*, 16102-16110; *ibid.*, **2006**, *110*, 24276-24276.

[45] Chou, K. C. Review: Structural bioinformatics and its impact to biomedical science. *Curr. Med. Chem.,* **2004**. *11*. 2105-2134.

[46] Chou, K. C. Modelling extracellular domains of GABA-A receptors: subtypes 1, 2, 3, and 5. *Biochem. Biophys. Res. Commun.,* **2004**, *316*, 636-642.

[47] Chou, K. C. Molecular therapeutic target for type-2 diabetes. *J. Proteome Res.,* **2004**, *3*, 1284-1288.

[48] Ban, H. S.; Usui, T.; Nabeyama, W.; Morita, H.; Fukuzawa, K.; Nakamura, H. Discovery of Boron-conjugated 4-Anilinoquinazoline as a Prolonged Inhibitor of EGFR Tyrosine Kinase. *Org. Biomol. Chem.,* **2009**, *7*, 4415-4427.

[49] Chou, K. C.; Wei, D. Q.; Zhong, W. Z. Binding mechanism of coronavirus main proteinase with ligands and its implication to drug design against SARS. (Erratum: ibid., 2003, Vol.310, 675). *Biochem. Biophys. Res. Comm.,* **2003**, *308*, 148-151.

[50] He, Z. S.; Zhang, J.; Shi, X. H.; Hu, L. L.; Kong, X. G.; Cai, Y. D.; Chou, K. C. Predicting drug-target interaction networks based on functional groups and biological features. *PLoS One,* **2010**, 5, e9603.

[51] Chou, K. C.; Wei, D. Q.; Du, Q. S.; Sirois, S.; Zhong, W. Z. Review: Progress in computational approach to drug development against SARS. *Curr. Med. Chem.,* **2006**, *13*, 3263-3270.

[52] Chou, K. C. Energy-optimized structure of antifreeze protein and its binding mechanism. *J. Mol. Biol.,* **1992**, *223*, 509-517.

[53] Chou, K. C.; Jones, D.; Heinrikson, R. L. Prediction of the tertiary structure and substrate binding site of caspase-8. *FEBS Lett.,* **1997**, *419*, 49-54.

[54] Chou, K. C. Coupling interaction between thromboxane A2 receptor and alpha-13 subunit of guanine nucleotide-binding protein. *J Proteome Res.,* **2005**, *4*, 1681-1686.

[55] Wang, J. F.; Wei, D. Q.; Li, L.; Zheng, S. Y.; Li, Y. X.; Chou, K. C. 3D structure modeling of cytochrome P450 2C19 and its implication for personalized drug design. *Biochem. Biophys. Re.s Commun.,* (Corrigendum: ibid, 2007, Vol. 357, 330), **2007**, *355*, 513-519.

[56] Li, L.; Wei, D. Q.; Wang, J. F.; Chou, K. C. Computational studies of the binding mechanism of calmodulin with chrysin. *Biochem. Biophys. Res. Comm.,* **2007**, *358*, 1102-1107.

[57] Wang, J. F.; Wei, D. Q.; Lin, Y.; Wang, Y. H.; Du, H. L.; Li, Y. X.; Chou, K. C. Insights from modeling the 3D structure of NAD(P)H-dependent D-xylose reductase of Pichia stipitis and its binding interactions with NAD and NADP. *Biochem. Biophys. Res. Comm.,* **2007**, *359*, 323-329.

[58] Gu, R. X.; Gu, H.; Xie, Z. Y.; Wang, J. F.; Arias, H. R.; Wei, D. Q.; Chou, K. C. Possible drug candidates for Alzheimer's disease deduced from studying their binding interactions with alpha7 nicotinic acetylcholine receptor. *Med. Chem.,* **2009**, 5, 250-262.

[59] Wang, J. F.; Yan, J. Y.; Wei, D. Q.; Chou, K. C. Binding of CYP2C9 with diverse drugs and its implications for metabolic mechanism. *Med. Chem.,* **2009**, *5*, 263-270.

[60] Wang, J. F.; Wei, D. Q.; Chen, C.; Li, Y.; Chou, K. C. Molecular modeling of two CYP2C19 SNPs and its implications for personalized drug design. *Protein Pept. Lett.,* **2008**, *15*, 27-32.

[61] Case, D. A.; Darden, T. A.; Cheatham, T. E.; Simmerling, III, C. L.; Wang, J.; Duke, R. E.; Luo, R.; Walker, R. C.; Zhang, W.; Merz, K. M.; Roberts, B. P.; Wang, B.; Hayik, S.; Roitberg, A.; Seabra, G.; Kolossváry, I.; Wong, K. F.; Paesani, F.; Vanicek, J.; Wu, X.; Brozell, S. R.; Steinbrecher, T.; Gohlke, H.; Cai, Q.; Ye, X.; Wang, J.; Hsieh, M.-J.; Cui, G.; Roe, D. R.; Mathews, D. H.; Seetin, M. G.; Sagui, C.; Babin, V.; Luchko, T.; Gusarov, S.; Kovalenko, A.; Kollman, P. A. AMBER 11. University of California: San Francisco, **2010**.

[62] Nakano, T.; Kaminuma, T.; Sato, T.; Fukuzawa, K.; Akiyama, Y.; Uebayasi, M.; Kitaura, K. Frgment Molecular Orbital Method: Use of Approximate Electrostatic Potential. *Chem. Phys. Lett.,* **2002**, *351*, 475-480.

[63] Mochizuki, Y.; Nakano, T.; Koikegami, S.; Tanimori, S.; Abe, Y.; Nagashima, U.; Kitaura, K. A parallelized integral-direct second-order Møller–Plesset perturbation theory method with a fragment molecular orbital scheme. *Theor. Chem. Acc.,* **2004**, *112*, 442-452.

[64] Mochizuki, Y.; Koikegami, S.; Nakano, T.; Amari, S.; Kitaura, K. Large scale MP2 calculations with fragment molecular orbital scheme. *Chem. Phys. Lett.,* **2004,** *396*, 473-479.

[65] Grimme, S. J. Improved second-order Møller–Plesset perturbation theory by separate scaling of parallel- and antiparallel-spin pair correlation energies. *Chem. Phys.,* **2003**, *118*, 9095-9102.

[66] Hill, J. G.; Platts, J. A. Spin-Component Scaling Methods for Weak and Stacking Interactions. *Phys. Chem. Chem. Phys.,* **2006**. *8*. 4072-4078.

[67] Sawada, T.; Fedorov, D. G.; Kitaura, K. Structural and Interaction Analysis of Helical Heparin Oligosaccharides with the Fragment Molecular Orbital Method. *Int. J. Quantum Chem.,* **2009**, *109*, 2033-2045.

[68] ABINIT-MP ver 4.3 and BioStation Viewer ver. 12.0 is available from the website of RSS21 project: http://www.ciss.iis.u-tokyo.ac.jp/dl.

[69] CLUSTALW version 1.83: http://clustalw.ddbj.nig.ac.jp

Received: October 11, 2010 **Revised: December 16, 2010** **Accepted: December 18, 2010**